

# Slab buckling as a driver for rapid oscillations in plate motion and subduction rate

Erik van der Wiel<sup>1</sup>, Jakub Pokorny<sup>2</sup>, Hana Cizkova<sup>3</sup>, Wim Spakman<sup>1</sup>, Arie van den Berg<sup>1</sup>, and Douwe J.J. van Hinsbergen<sup>1</sup>

<sup>1</sup>Utrecht University

<sup>2</sup>Charles University

<sup>3</sup>Charles University, Faculty of Mathematics and Physics

November 22, 2023

## Abstract

Plate tectonics is primarily driven by the constant gravitational pull of slabs where dense oceanic lithosphere sinks into the mantle at subduction zones. Under stable plate boundary configurations, changes in plate motion are then thought to occur gradually. Surprisingly, recent high-resolution Indian plate reconstructions revealed rapid (2-3 Ma) plate velocity oscillations of  $\pm 50\%$ . Here we show, through numerical experiments, that the buckling of slabs in the mantle transition zone causes such oscillations. This buckling results from the deceleration of slabs as they sink into the lower mantle. The amplitude and period of buckling-associated oscillations depend on average subduction velocity and transition zone accommodation space. The oscillations also affect the upper plate which may explain enigmatic observations of episodic deformation and fluid flow in subduction-related orogens. We infer that the slab pull that drives plate tectonics is generated in just the top few hundred kilometers of the mantle.

## Hosted file

980052\_0\_art\_file\_11610672\_s4fdkz.docx available at <https://authorea.com/users/702747/articles/688567-slab-buckling-as-a-driver-for-rapid-oscillations-in-plate-motion-and-subduction-rate>

# Slab buckling as a driver for rapid oscillations in plate motion and subduction rate

Erik van der Wiel<sup>1\*</sup>, Jakub Pokorný<sup>2\*\*</sup>, Hana Čížková<sup>2</sup>, Wim Spakman<sup>1</sup>, Arie P. van  
den Berg<sup>1</sup>, Douwe J.J. van Hinsbergen<sup>1</sup>

1. Utrecht University

2. Charles University Prague

*\*Corresponding authors: Erik van der Wiel (e.vanderwiel@uu.nl) and Jakub Pokorny  
(jaakubpokorny@gmail.com).*

† These authors contributed equally to this work

*For: AGU advances*

## 19 Abstract

20 Plate tectonics is primarily driven by the constant gravitational pull of slabs where dense  
21 oceanic lithosphere sinks into the mantle at subduction zones. Under stable plate boundary  
22 configurations, changes in plate motion are then thought to occur gradually. Surprisingly,  
23 recent high-resolution Indian plate reconstructions revealed rapid (2-3 Ma) plate velocity  
24 oscillations of  $\pm 50\%$ . Here we show, through numerical experiments, that the buckling of  
25 slabs in the mantle transition zone causes such oscillations. This buckling results from the  
26 deceleration of slabs as they sink into the lower mantle. The amplitude and period of  
27 buckling-associated oscillations depend on average subduction velocity and transition zone  
28 accommodation space. The oscillations also affect the upper plate which may explain  
29 enigmatic observations of episodic deformation and fluid flow in subduction-related  
30 orogens. We infer that the slab pull that drives plate tectonics is generated in just the top  
31 few hundred kilometers of the mantle.

## 32 Plain-Language Summary

33 Motions of tectonic plates are relatively stable over 10s of millions of years and are mainly driven by  
34 the gravitational pull of the subducting part of the plate. However, new data from the Indian plate  
35 shows that these velocities may vary rapidly in magnitude. Deeper in the Earth's mantle the  
36 deceleration of subducted plates, as they encounter more resistance, causes them to fold. Our  
37 models show that this folding can cause the rapid variations of plate motion at short (2-3 million  
38 year) timescales and that these variations may also cause episodic deformation of the overriding  
39 plate. We propose new insights in the range (depth) at which the gravitational pull of a subducting  
40 plate may still influence its plate motion.

41

## 42 1. Introduction

43 Plate kinematic reconstructions provide the quantitative constraints that underpin our  
44 understanding of the driving and resisting forces of plate tectonics: primarily slab pull and to a lesser  
45 extent ridge push as driving forces (Forsyth & Uyeda, 1975; Lithgow-Bertelloni & Richards, 1998),  
46 and mantle drag as either driving or resisting plate motion (particularly by continental keels or  
47 slabs), and the resistance on subduction interfaces, as main additional forces (Behr & Becker, 2018;  
48 Coltice et al., 2019; Spakman et al., 2018). An important constraint on plate reconstruction and  
49 relative plate motions since the Mesozoic is provided by marine magnetic anomalies that reveal

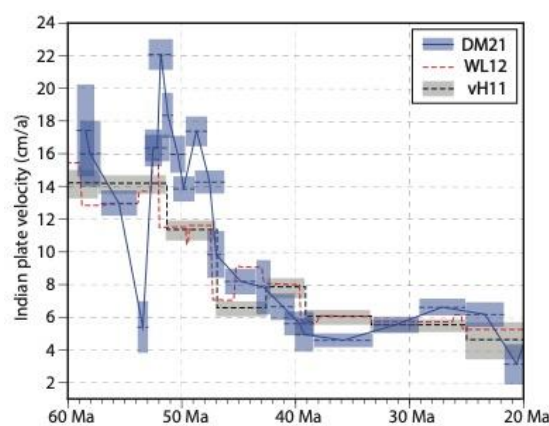
50 plate motion change on various temporal scales. Reconstructions of major ocean basins usually  
51 provide one average Euler pole (plate motion data point) for stages of 3-10 Ma (e.g. Müller et al.,  
52 2019), even though often more magnetic anomalies can be present in such stages. Such  
53 reconstructions reveal gradually changing plate motions on tens of millions of year time scales with  
54 occasional sudden cusps in plate motion between stages (Dobrovine et al., 2012; Müller et al.,  
55 2022; Torsvik et al., 2008). Gradual plate motion changes can be explained by changes in slab pull for  
56 example due to slow age variation of subducting lithosphere (Goes et al., 2011; Sdrolias & Müller,  
57 2006), or in the lubrication of plate contacts (Behr & Becker, 2018). Cusps may correspond to  
58 changes in contributing forces through e.g., changes in slab pull due to subduction initiation or arrest  
59 (Gürer et al., 2022; Hu et al., 2022), by slab detachment (Bercovici et al., 2015) or resistance to  
60 subduction of large oceanic plateaus (Knesel et al., 2008), the arrival of a mantle plume-head that  
61 may lubricate or push plates (van Hinsbergen et al., 2011; van Hinsbergen et al., 2021), or to the  
62 decrease of a plate area through breakup (e.g., Wortel & Cloetingh, 1981). Only recently, high-  
63 resolution (~0.5-1 Ma) plate kinematic reconstructions of India-Africa spreading during the Eocene  
64 (DeMets & Merkouriev, 2021) revealed surprisingly variable ocean spreading kinematics.

65 It has long been known that the spreading rate between India and Africa, and the  
66 convergence rate between India and Asia, between ~65 and ~50 Ma, was very high, close to 20 cm/a  
67 (Patriat & Achache, 1984; van Hinsbergen et al., 2011). Those estimates were based on about one  
68 Euler pole every ~5 Ma. White & Lister (White & Lister, 2012) suspected that shorter-wavelength  
69 plate velocity oscillations may have occurred although being smoothed out in existing global plate  
70 tectonic reconstructions. Their suspicion was recently corroborated by the high-resolution magnetic  
71 anomaly study of (DeMets & Merkouriev, 2021), which revealed that the period of high India-Asia  
72 convergence rate contained rapid oscillations with an amplitude 10 cm/a or more at a period of 6-8  
73 Ma (Figure 1). Such plate motion variations suggest that a hitherto unrecognized process plays a role  
74 that causes oscillating changes in either slab pull, or friction, or both that perhaps becomes more  
75 pronounced with higher rates of subducting plate motion.

76 Subducting plate motions and changes therein must be accommodated in the underlying  
77 mantle. Correlations between imaged mantle structure and the global geological record of  
78 subduction show that the remnants of detached slabs in the lower mantle sink with rates of ~1-1.5  
79 cm/a, almost regardless of the rate at which they subducted at a trench (Butterworth et al., 2014;  
80 Van Der Meer et al., 2010; Van der Meer et al., 2018). Therefore, subducting slabs eventually  
81 decelerate from plate tectonic rates (up to 20-25 cm/a (Hu et al., 2022; Zahirovic et al., 2015) to  
82 average lower mantle sinking rates of <1.5 cm/a. To accommodate this requires some form of slab  
83 shortening or thickening. Subduction modelling revealed that this deceleration naturally leads to

84 slab thickening, which could occur in the mantle transition zone through slab buckling (Goes et al.,  
85 2017; Ribe et al., 2007; Sigloch & Mihalynuk, 2013). Later, detailed tomographic analyses of slabs in  
86 the mantle transition zone and in the top of the lower mantle confirmed that they are systematically  
87 buckled (Chen et al., 2019; Wu et al., 2016). Tomography of the lower mantle below India has  
88 revealed a major slab that is widely interpreted to represent the subducted Neotethys ocean, and  
89 that also contains the lithosphere that subducted between 65 and 50 Ma (Parsons et al., 2021;  
90 Qayyum et al., 2022; Replumaz et al., 2004; Van der Voo et al., 1999). The enormous volume of this  
91 slab requires that it was drastically thickened, and while tomographic detail so far has not been able  
92 to resolve internal structure, the documentation that slabs buckle during thickening elsewhere  
93 (Chen et al., 2019; Wu et al., 2016) makes it feasible that this process also played a role here. Such  
94 buckling, which potentially may become more pronounced with faster subduction, makes slabs fold  
95 backward and forward, creating an oscillating slab dip and slab motion (Billen & Arredondo, 2018;  
96 Čížková & Bina, 2013; Garel et al., 2014; Holt et al., 2015; Lee & King, 2011; Schellart, 2005; Xue et  
97 al., 2022). Here, we hypothesize that pronounced slab buckling causes the rapid, large-amplitude  
98 Eocene plate motion fluctuations of India.

99 To test this hypothesis, we conduct numerical experiments with decoupled, freely  
100 subducting plates that buckle in the mantle transition zone, creating periodically changing plate  
101 motions (Pokorný et al., 2021). We evaluate under which conditions fluctuations such as those  
102 reported for the India plate may occur. We will discuss our results in terms of the implications for  
103 our understanding of the driving forces of plate tectonics, and how obtaining detailed marine  
104 magnetic anomaly records may aid improving the predictive power of plate tectonic reconstructions  
105 for applications to plate boundary deformation and magmatic or mineralization processes.



106

### 107 **Figure 1 – Indian plate motion history**

108 Indian plate velocity relative to Eurasia from 60 Ma ago to 20 Ma ago. Shown are the reconstructed  
109 velocities of the Indian plate from DM21 (DeMets & Merkouriev, 2021), WL12 (White & Lister, 2012)  
110 and vH11 (van Hinsbergen et al., 2011). Blue and grey rectangles indicate error margins in  
111 reconstructions and time interval spanned by each stage velocity.

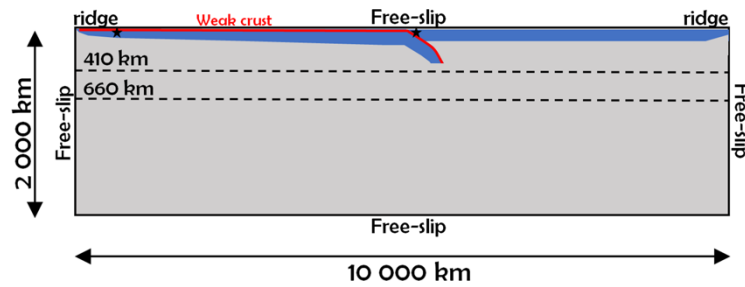


**Figure 2 – Model setup**

Model domain is 10 000 km wide and 2000 km deep. Dashed lines indicate major phase transitions at 410 and 660 km depth. Red line positioned at the top of the subducting slab indicates a 10 km thick weak crustal layer, effectively separating the plates. Two black asterisks represent tracers used to track the velocity of the subducting plate and overriding plate. Free slip boundary condition is prescribed on all boundaries.

## 2. Methods and model setup

A set of partial differential equations in an extended Boussinesq approximation (Ita & King, 1994) (EBA) is used to describe our numerical model of subduction. These equations are solved by a finite element method implemented in the SEPRAN package (Segal & Praagman, 2005; van den Berg et al., 2015). Our model domain is represented by a 2D box 10,000 km wide and 2,000 km deep (Figure 2). The subducting plate stretches from the ridge in the upper left corner to the trench in the middle of the upper surface. The initial temperature distribution in the subducting plate follows a half-space model followed by an adiabatic profile with a potential temperature of 1573 K beneath it.

We carried out two sets of simulations with similar matching parameters. The first set with an overriding plate that is allowed to move freely (subduction with possible rollback), while the second set features a fixed overriding plate (stationary trench – restricted rollback). Figure 3 illustrates time evolution of a reference model for both sets of simulations. In these reference models we assume a subducting and overriding plate age of 100 Ma at the trench and the viscosity of the crustal decoupling layer of  $10^{20} Pa \cdot s$ .

Models of the first set have a mobile overriding plate with a ridge in the upper right corner. The rollback of trench induces the motion of the entire overriding plate towards the left, which is facilitated by the presence of a hot and low-viscosity mid-ocean ridge. The second set of models has a stagnant overriding plate with an age increasing from approximately  $\sim 17$  Ma at the right-hand side to 100 Ma (i.e., for the reference model) at the trench. Cold and thus strong overriding plates cannot move to the left because of the impermeable free slip condition on the right vertical boundary. Therefore, rollback is prohibited and the trench remains stagnant during the model run. We evaluated the effects of the age of the subducting and overriding plates (Capitanio et al., 2010; Garel et al., 2014) – we tested ages at the trench ranging from 50 Ma to 200 Ma.

142 To obtain an initial slab with sufficient negative buoyancy that would facilitate subduction,  
143 we first execute a short kinematic run to develop the slab tip to a depth of approximately 200 km.  
144 Within this kinematic prerun a constant convergence velocity of 2.5 cm/a is prescribed on the top of  
145 the subducting plate. After 6 Ma the kinematic boundary condition is turned off and an impermeable  
146 free slip is prescribed on all boundaries.

147 Top and bottom model boundaries are considered isothermal with respective temperatures  
148 of 273 K and 2132 K while the vertical boundaries have zero heat flux. Thermal diffusivity is constant  
149  $10^{-6} \text{ m}^2 \text{ s}^{-1}$  while thermal expansivity is depth dependent (Katsura et al., 2009) and decreases  
150 from  $3 \times 10^{-5} \text{ K}^{-1}$  at the surface to  $1.2 \times 10^{-5} \text{ K}^{-1}$  at the bottom of the model domain (Hansen  
151 et al., 1993).

152 We consider the major mantle phase transitions: the polymorphous exothermic transition of  
153 forsterite to wadsleyite at 410 km depth and the endothermic transition of ringwoodite to  
154 bridgmanite and periclase at a depth of 660 km with their associated petrological density contrasts  
155 (Supplementary Table 1). These are incorporated through the harmonic parameterization (Čížková et  
156 al., 2007) of a phase function (Christensen & Yuen, 1985). We performed a parametric study where  
157 we varied the values of Clapeyron slopes in a usually accepted range ( $\gamma_{410} = 1 - 3 \text{ MPa/K}$ ,  
158  $\gamma_{660} = -2.5 - (-1.5) \text{ MPa/K}$ ). All these models result in quasiperiodic buckling of the slab. The  
159 strengths of the phase transitions control slab dip angle and related rollback velocity, the ability to  
160 penetrate the lower mantle as well as slab viscosity in the transition zone. These factors than affect  
161 observed periods of the oscillations that vary between  $\sim 10 - 20 \text{ Ma}$ . Based on this parametric study  
162 we chose the values of Clapeyron slopes of 3 MPa/k and -1.5 MPa/K for the 410 km and 660 km  
163 phase transitions. These values were chosen to accommodate realistic average subduction velocities  
164 (Zahirovic et al., 2015) with fast plate velocity oscillations (DeMets & Merkouriev, 2021) while still  
165 agreeing with in-situ X-ray diffraction experiments and thermodynamic estimates (Bina & Helffrich,  
166 1994; Katsura et al., 2004; Morishima et al., 1994; Su et al., 2022).

167 To evaluate the subducting plate velocity and trench retreat velocity in our models we use  
168 two passive particles, one initially positioned in the subcrustal lithosphere of the subducting plate  
169 ( $\sim 4600 \text{ km}$  left of the trench) and the other one in the overriding plate close to the trench (Figure 2).

170

## 171 **2.1 Rheological description**

172 Our subduction model incorporates crustal and mantle material. A low-viscosity crustal layer  
173 facilitating mechanical decoupling of the subducting and overriding plate is initially positioned along  
174 the top of the subducting plate and within the subduction channel (Figure 2). Crustal material is  
175 tracked using 2 million tracers prescribed in the crust and its closest vicinity. The initial thickness of  
176 the crustal layer is 10 km.

177 Upper mantle material is described by a composite rheology model (Čížková et al., 2002; van  
 178 den Berg et al., 1993) combining dislocation creep, diffusion creep and a power-law stress limiter  
 179 which effectively approximates the Peierls creep (Androvičová et al., 2013). In the diffusion and  
 180 dislocation creep equations (equations 1 and 2), the pressure and temperature dependence of  
 181 viscosity follows Arrhenius law:

$$183 \quad \eta_{diff} = A_{diff}^{-1} \exp\left(\frac{E_{diff} + pV_{diff}}{RT}\right) \quad (1)$$

$$184 \quad \eta_{disl} = A_{disl}^{-1/n} \dot{\epsilon}_{||}^{(1-n)/n} \exp\left(\frac{E_{disl} + pV_{disl}}{nRT}\right) \quad (2)$$

$$185 \quad \eta_y = \sigma_y \dot{\epsilon}_y^{-(1/n_y)} \dot{\epsilon}_{||}^{(1/n_y)-1} \quad (3)$$

$$186 \quad \frac{1}{\eta_{eff}} = \frac{1}{\eta_{diff}} + \frac{1}{\eta_{disl}} + \frac{1}{\eta_y} \quad (4)$$

187

188 Here  $A_{diff/disl}$ ,  $E_{diff/disl}$ ,  $V_{diff/disl}$  are pre-exponential parameter, activation energy, activation  
 189 volume for diffusion and dislocation creep,  $\dot{\epsilon}_{||}$  is the second invariant of the strain rate tensor and  
 190  $n$  is the power-law exponent of the dislocation creep. A power law stress limiter viscosity is  
 191 parametrized through the yield stress  $\sigma_y$ , reference strain rate  $\dot{\epsilon}_y$  and a power-law exponent  $n_y$ ,  
 192 which is set to 10 in our models (equation 3). Assuming unique stress, individual creep mechanism  
 193 viscosities are combined into the effective viscosity through equation 4.

194 The lower mantle deformation is assumed to be mainly through diffusion creep (Karato et  
 195 al., 1995), therefore we take  $\eta_{eff} = \eta_{diff}$  in the lower mantle. Prefactor  $A_{diff}$  and activation  
 196 parameters of lower mantle diffusion creep are based on slab sinking speed analysis (Čížková et al.,  
 197 2012).

198 The crust in our models is mostly assumed to have constant viscosity in a range of  
 199  $\eta_c = 5 \times 10^{19} - 5 \times 10^{20} \text{ Pa s}$ . We have also conducted several tests with the composite nonlinear  
 200 rheology of the crust (Pokorný et al., 2021) combining dislocation creep (Ranalli, 1995) and a Byerlee  
 201 type deformation (Karato, 2008) as an approximation of the brittle failure (pseudoplastic  
 202 deformation). In these models, dislocation creep viscosity follows equation 5 (similar to equation 2),  
 203 but the parameters  $A_c$ ,  $E_c$ ,  $V_c$  and  $n_c$  differ from mantle parameters of equation 2 – see table.

204

$$205 \quad \eta_{disl}^c = A_c^{-1/n_c} \dot{\epsilon}_{||}^{(1-n_c)/n_c} \exp\left(\frac{E_c + pV_c}{n_c RT}\right) \quad (5)$$

206

207 Pseudoplastic deformation limits the maximum stress in the crust to  $\sigma_y^c$ , where this stress  
 208 limit increases with lithostatic pressure  $p$  through equation 6, here  $\tau_c$  is the cohesion and  $\mu$  is the



209 friction coefficient. The pseudoplastic viscosity  $\eta_{pl}$  is then defined by equation 7 and the effective  
210 crustal viscosity is given by equation 8.

211

$$212 \quad \sigma_y^c = \tau_c + \mu p, \quad (6)$$

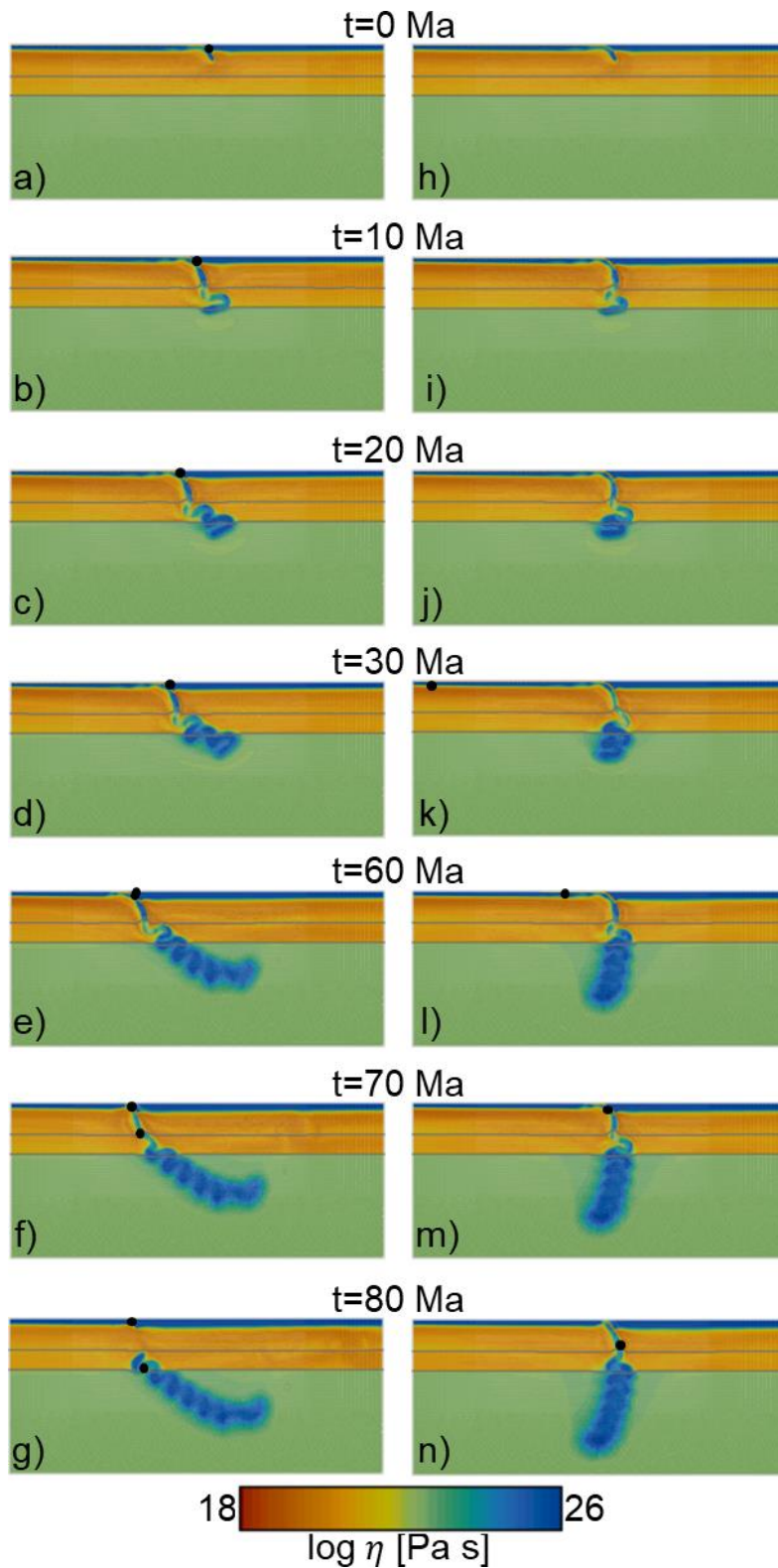
$$213 \quad \eta_{pl} = \frac{\sigma_y^c}{2\dot{\epsilon}_{||}}. \quad (7)$$

$$214 \quad \frac{1}{\eta_{eff}^c} = \frac{1}{\eta_{disl}^c} + \frac{1}{\eta_{pl}^c}. \quad (8)$$

### 215 3. Results

216 We conducted experiments in a 2D numerical model of subduction (see methods). The  
217 rheology of the upper and lower mantle (Čížková & Bina, 2013, 2019; Čížková et al., 2012) was  
218 chosen to accommodate typical subduction velocities (Zahirovic et al., 2015) that in the upper  
219 mantle exceed the inferred lower mantle average slab sinking rates (Van der Meer et al., 2018). This  
220 mantle rheology leads to slab shortening and buckling in the upper-to-lower mantle transition zone  
221 (MTZ). We experimented with varying lithospheric ages to assess the effect of varying oceanic  
222 lithosphere thickness, and with varying crustal viscosities to assess the effect of average plate  
223 motion on the amplitude and period of the plate motion. We conducted one group of experiments,  
224 with a free overriding plate which leads to slab rollback and results in low angle buckling with  
225 multiple buckles (partly) present in above the 660 km discontinuity, and lower net lower mantle slab  
226 sinking rates (Figure 3a-g). Another group of experiments implements a fixed overriding plate that  
227 suppresses the development of rollback, such that subduction occurs at a mantle-stationary trench  
228 (Figure 3h-n). This generates buckling into a near-vertical slab-pile (Běhounková & Čížková, 2008)  
229 that slowly sinks into the lower mantle leaving at any time only one buckle present above the 660  
230 km discontinuity.

231 Slab shortening occurs through the combined resistance of the more viscous lower mantle  
232 and the endothermic phase change at the 660 km boundary, while the shallower part of the slab is  
233 continuously pulled by the exothermic phase change at 410 km (see methods). Buckling of the  
234 shortening slab is influenced by the non-linear rheology of the slab that results from the presence of  
235 a crust and lithospheric mantle layer (Pokorný et al., 2021). We assess the horizontal velocity of the  
236 subducting plate  $V_{SP}$  and upper plate  $V_{UP}$  as an effect of lithospheric thickness (corresponding to the  
237 age of lithosphere at the trench) or through weakening subduction interfaces (crustal viscosity) to  
238 evaluate causal relationships between subduction dynamics and oscillating plate motions.



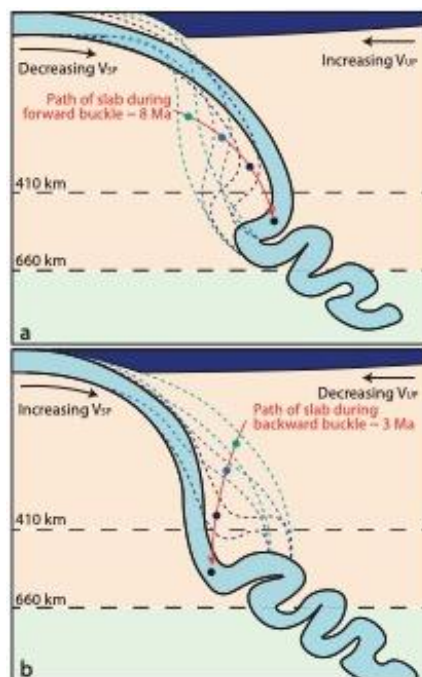
239

240 **Figure 3 – Time evolution of the reference models**

241 Zoomed-in viscosity snapshots (4800x2000 km) of the model for 80 Ma of model time. Grey lines  
 242 indicate position of the major phase transition at 410 and 660 km depth with the values of  
 243 Clapeyron slopes of 3 and -1.5 MPa/K, respectively. Black dots are reference points used to calculate  
 244 plate velocities. A-G) Reference model with free moving overriding plate resulting in trench retreat  
 245 and an inclined slab in the lower mantle. H-N) Reference model with a stationary trench creating a  
 246 vertical lower mantle slab.

### 247 3.1 Slab buckling in the reference models

248 Figure 3 shows two reference experiments for the model setups with and without roll-back.  
249 These have a crustal viscosity of  $10^{20} \text{ Pa} \cdot \text{s}$  and overriding and subducting plate ages at the trench  
250 of 100 Ma. In the model with a mobile overriding plate (Figure 3 a-g), the slab undergoes a rapid,  
251 vertical descent through the upper mantle and the tip reaches the 660 km discontinuity after  
252 approximately 5 Ma model time (Supplementary Movie – panel A). The slab in the transition zone  
253 experiences down-dip compression which leads to (nonlinear) rheological weakening, causing the  
254 slab to buckle forwards (Figure 4a) (i.e., towards the overriding plate) over the trapped tip that  
255 started to penetrate the 660 km discontinuity. Next, the slab buckles backward (i.e. towards the  
256 downgoing plate). This leads to an episode of roll-back and short-lived  $V_{SP}$  increase until the slab is  
257 almost vertically orientated at  $t = 11 \text{ Ma}$  (Figure 4b). This is followed by the initiation of a second  
258 forward buckle, folding the slab over its deeper part in the MTZ, between  $t = 11 \text{ Ma}$  and 18 Ma  
259 (Supplementary movie – panel A), associated with rollback and a decrease of  $V_{SP}$  and increase of  $V_{UP}$   
260 (Figure 4b & 5a). This forward buckle starts tightening at  $t = 18 \text{ Ma}$ , inducing the next backward  
261 buckle which is followed by a rapid increase of  $V_{SP}$  up to  $12 \text{ cm/a}$ , accompanied by a decrease of  $V_{UP}$   
262 to almost  $0 \text{ cm/a}$  (Figure 5a). At  $t = 20 \text{ Ma}$  the next forward buckle initiated (Figure 3c), resulting again  
263 in an episode of rollback with decreasing  $V_{SP}$  and increasing  $V_{UP}$  (Figure 4a & 5a).



264 **Figure 4 – Illustrated effect of slab buckling on upper mantle slab geometry**  
265 A cartoon illustrating forward (A) and backward (B) slab buckling as result of the interplay of the slab  
266 with the phase transitions and the lower mantle. During forward buckling the slab in the MTZ  
267 advances while the trench retreats, accompanied by a decreasing  $V_{SP}$  and increasing  $V_{UP}$ . The  
268 backward buckle allows the slab to sink fast in the MTZ with a rapid increase of  $V_{SP}$ , while the trench  
269 stays mantle stationary. The backward buckles form faster than forward buckles, in about 3 versus 8  
270 Ma for our reference model.  
271

272 From here on, this process repeats itself quasi-periodically with new buckles forming  
273 approximately every 10 Ma (Figure 3c-f). This continuous subduction and rollback creates a buckled  
274 and thickened slab which slowly enters the lower mantle at an overall low-angle orientation (Figure  
275 3d-g). After 70 Ma and 5000 km of subduction, the weak crust that facilitates the modelled  
276 subduction (see methods) is entirely consumed, the subducting plate is locked to the overriding  
277 plate and subduction stops. The modelled slab detaches and sinks into the lower mantle at a rate of  
278  $\sim 1$  cm/a, on par with inferred and modelled lower mantle slab sinking rates (Čížková et al., 2012; Van  
279 der Meer et al., 2018). Throughout the experiment, and after 70 Ma of modelled convergence, the  
280 overriding plate and trench moved  $\sim 1000$  km in absolute motion, i.e., relative to the mantle,  
281 towards the subducting plate.

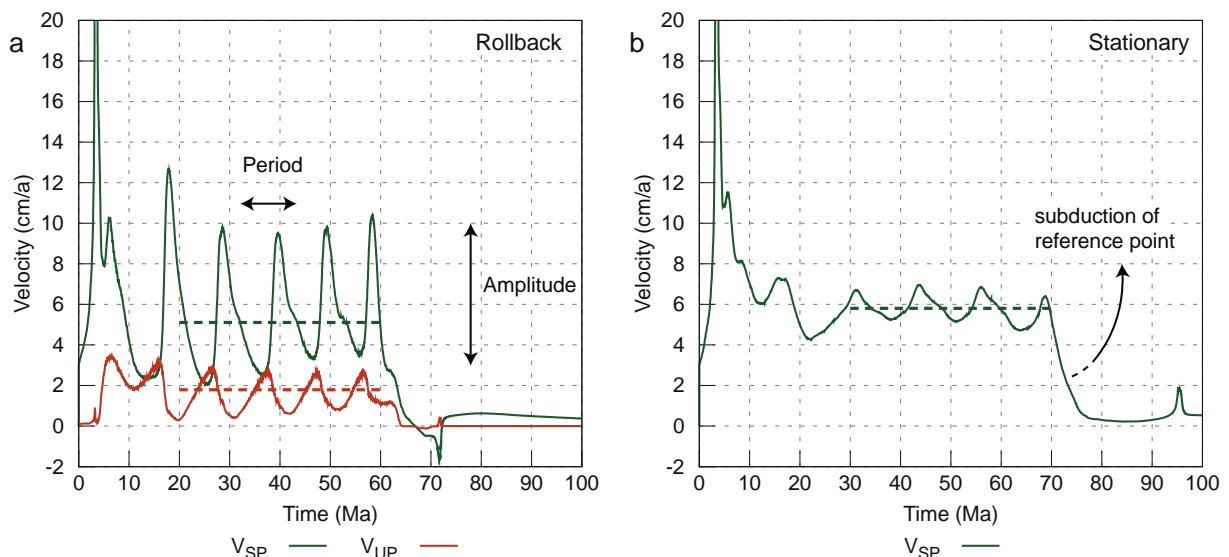
282 The model with a fixed overriding plate, which suppresses rollback (Figure 3 H-N), shows  
283 similar characteristics. The slab is compressed down-dip and rheologically weakened in the transition  
284 zone, also resulting in the formation of a second buckle at around  $t=10$  Ma (Figure 3i and  
285 Supplementary Movie – Panel B). The tightening of the buckle at the base of the upper mantle  
286 coincides with an increase in plate velocity around  $t=15$ Ma (Figure 5b). Due to the absence of  
287 rollback, the buckled slab is oriented vertically, like previously conceptualised ‘slab walls’ (Sigloch &  
288 Mihalyuk, 2013). The oscillations in  $V_{SP}$  are of lower amplitude, on the order of 2 cm/a, recurring in  
289 a  $\sim 12$  Ma period (Figure 5b). Absolute motion rates and oscillations therein of the subducting plate  
290 are similar to the scenario with roll-back but because the upper plate is fixed and roll-back does not  
291 add to the net convergence rate, subduction continued for  $\sim 90$  Ma in model time, after which, the  
292 modelled slab detached and descended through the lower mantle with similar rate as in the  
293 reference model with rollback.

294

### 295 **3.2 Plate motion oscillations caused by buckling**

296 The quasiperiodic buckling of the subducting plate in the MTZ causes oscillations in the  
297 subduction velocity for both types of models (Figure 5) and in the motion of the overriding plate in  
298 the models that allow for roll-back (Figure 5a). Periods of fast  $V_{SP}$  coincide with tightening of a buckle  
299 and steepening of the slab and correspond with minima in the  $V_{UP}$  (Figure 5). We represent the  
300 periodicity of these plate motions with an amplitude and period, which we calculate in a 40 Ma  
301 time-interval of steady-state oscillations after subduction initiation and initial descend of the slab to  
302 the mantle transition zone, and before the end of the experiment (Figure 5). In the reference model  
303 with rollback, the subducting plate moved between 20 and 60 Ma with an average  $V_{SP}$  of 5.1 cm/a  
304 while oscillating between  $\sim 2$  and 10 cm/a (Figure 5a). The average amplitude and period of the  $V_{SP}$   
305 oscillations are 6.8 cm/a and 9.8 Ma (Figure 5a). Motion of the rigid, undeformable overriding plate,

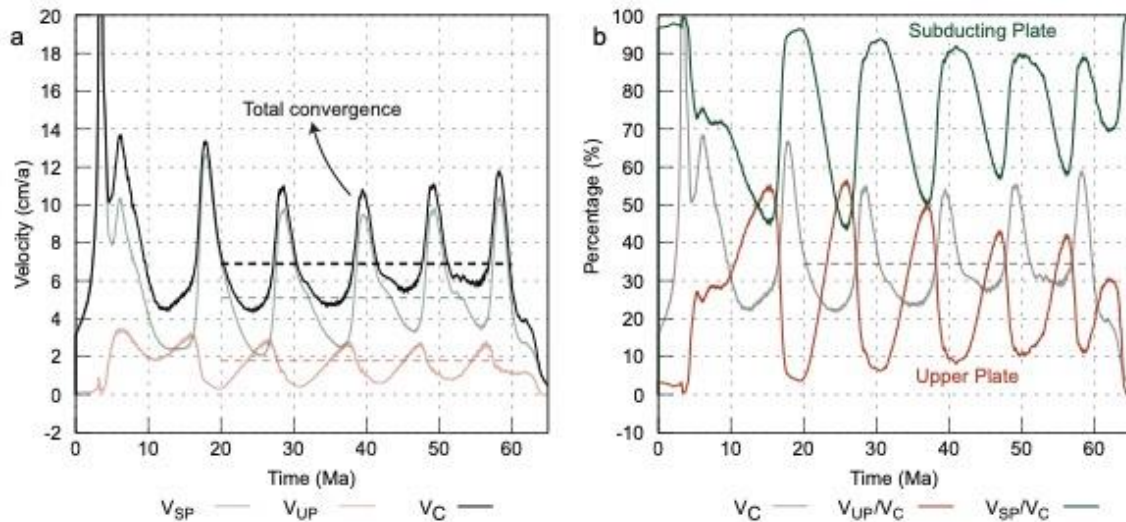
306 follows the oscillatory motion of the retreating trench. In the 20-60 Ma interval the overriding plate  
 307 has an average  $V_{UP}$  of 1.8 cm/a towards the subducting plate, with oscillations between ~0 and 3  
 308 cm/a (Figure 5a). Maxima in trench motion and  $V_{UP}$  coincide with minima in  $V_{SP}$ , both occurring  
 309 during formation of a new forward buckle and the associated shallowing of slab dip. During  
 310 tightening of the buckle, the slab rolls back from inclined to vertical, associated with a sharp rise in  
 311  $V_{SP}$ , this change in angle is associated with a temporally near-stationary trench, and a resulting  
 312 decrease in  $V_{UP}$  towards 0. The total convergence rate ( $V_C$ ) then also oscillates (Figure 6a), with an  
 313 amplitude of 6 cm/a, about 1 cm/a smaller than the amplitude of  $V_{SP}$ . The motion of the subducting  
 314 plate accounts for 50-100% of the total convergence, while the overriding plate is only responsible  
 315 for 50-0% (Figure 6b). The highest contribution of trench motion to the convergence occurs during  
 316 periods of minimal  $V_{SP}$ .  
 317



318  
 319  
 320  
 321  
 322  
 323  
 324  
 325  
 326

**Figure 5 – Plate motion oscillations**

Temporal evolution of the plate motions in both reference models. A) Subduction velocity and overriding plate motion of the reference model with rollback,  $V_{SP}$  oscillates between 2 and 10 cm/a and  $V_{UP}$  between 0 and 3 cm/a. The reference point subducts at  $t = 60$  Ma and slab detachment occurs around  $t = 70$  Ma. B) Similar as in A but for the reference model with a stationary trench, subduction of the reference point occurs at  $t = 70$  Ma and slab detachment at  $t = 90$  Ma. The dashed lines indicate the average velocity, which is calculated over the shown 40 Ma time-interval.



327  
328 **Figure 6 – Total convergence rate**

329 A) Total convergence rate ( $V_C = V_{SP} + V_{UP}$ ) of the reference model with rollback showing smaller  
330 amplitudes in the oscillations, red and green lines are the same as in Figure 5A. B) Relative  
331 percentages of the total convergence rate for both the subducting plate (green; 100-50%) and  
332 overriding plate (orange; 50-0%). Grey line is the same as in A, and uses the y-axis of A.  
333

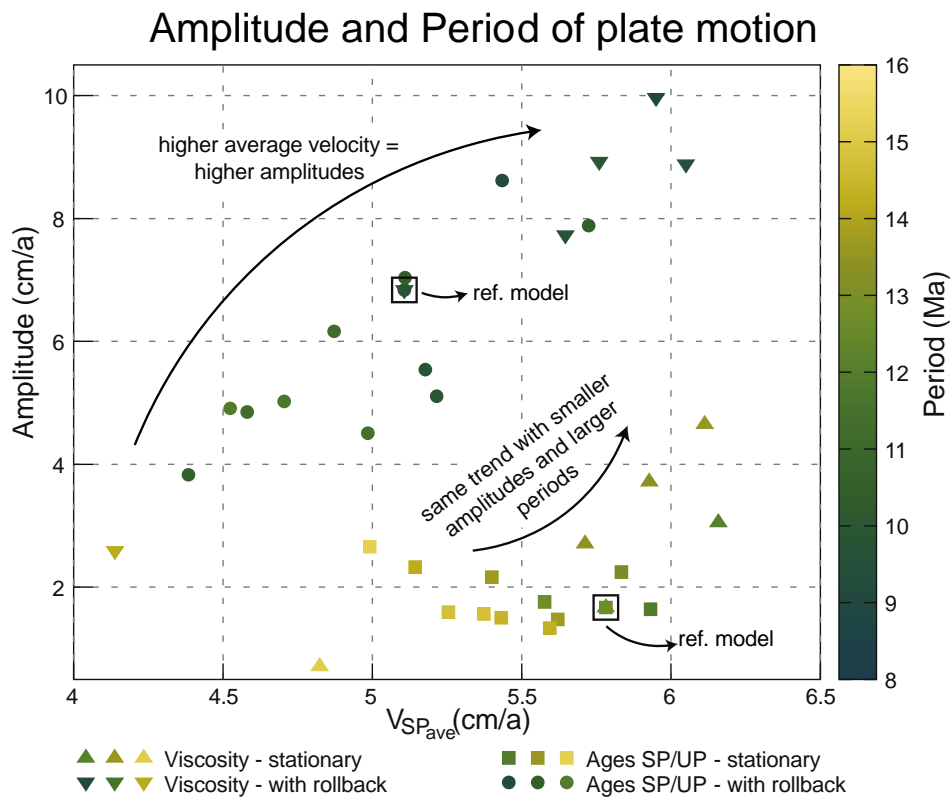
334 The reference model with a fixed overriding plate (Figure 3h-n), so with a mantle-stationary  
335 trench, also shows oscillations in  $V_{SP}$  (Figure 5b) caused by the buckling of the overall vertical slab in  
336 the MTZ. In the 40 Ma long time-interval (here, between 30-70 Ma) quasiperiodic buckling occurs  
337 with an average  $V_{SP}$  of 5.7 cm/a (Figure 5b), faster than the model with rollback. The oscillations in  
338  $V_{SP}$  occur with a period of 12.7 Ma and an amplitude of 1.6 cm/a. This amplitude is more than 4  
339 times lower than the amplitude of oscillations in the model with rollback. The freedom to roll back  
340 allows for much larger variation in slab dips, and results in higher amplitudes of plate motion  
341 oscillations, as well as a higher net convergence rate.

342

### 343 3.3 How subduction velocity controls plate motion oscillations

344 When lithosphere subducts at a rate of 5-6 cm/a as in our reference models, it can reach the  
345 660-discontinuity 13-11 Ma after passing the trench. Higher subduction rates decrease that time  
346 interval and increase the amount of subducted slab in the MTZ, creating an accommodation space  
347 problem. We performed numerical experiments to evaluate the effect of subduction speed on the  
348 formation of buckles and on oscillations in  $V_{SP}$ . We modified the subduction rate in our experiments  
349 in two ways. On the one hand, we performed experiments with constant crustal viscosity while  
350 varying the age of the overriding and subducting plates. Overriding plate age determines the length  
351 of the subduction interface, with larger interfaces giving more resistance against subduction,  
352 decreasing subduction velocity. Subducting plate age determines the negative buoyancy, with higher  
353 subduction velocities for older plates (Capitanio et al., 2011). On the other hand, we performed

354 experiments with constant lithosphere ages (100 Ma) while adopting a constant or a power-law  
 355 crustal viscosity, with lower viscosity yielding higher  $V_{SP}$  (e.g., Behr et al., 2022; see methods).



356

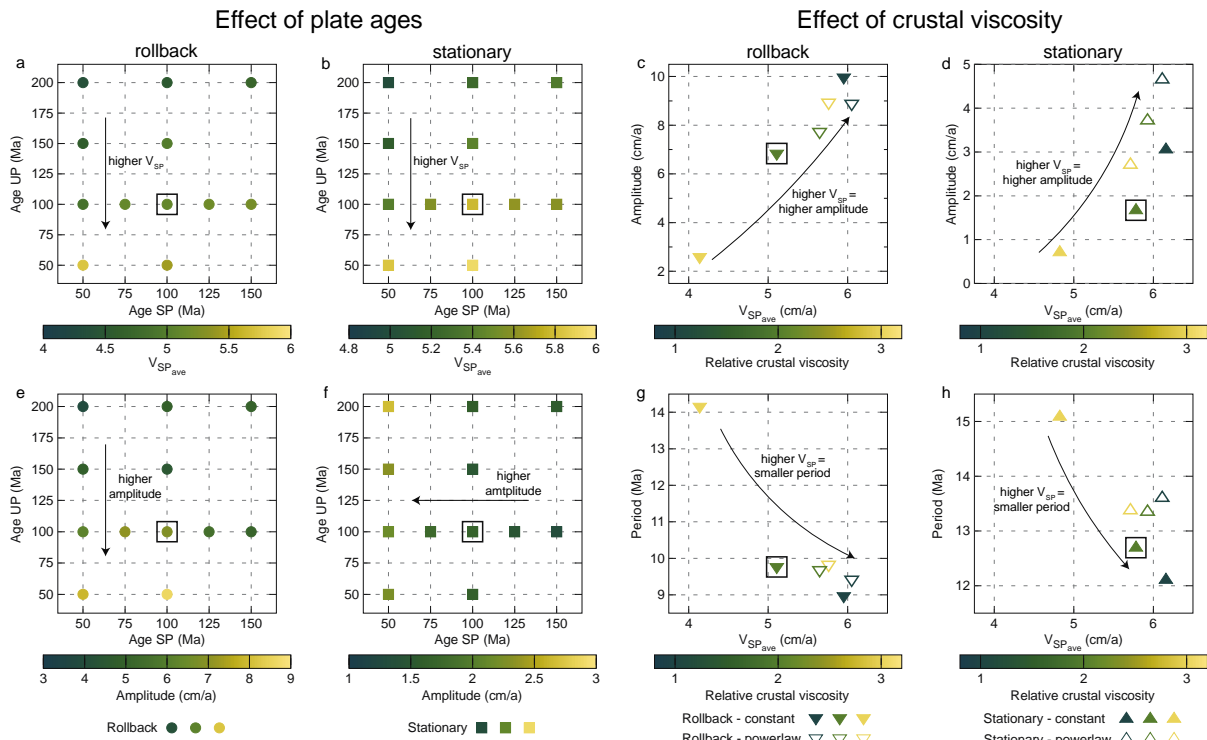
357 **Figure 7 – Amplitude and Period of the subducting plate motion**

358 Overview of all models showing the relation the amplitude and period (colour) of  $V_{SP}$  oscillations  
 359 have with the average  $V_{SP}$ . The four types of models shown are with a varying crustal viscosity and  
 360 rollback (triangles) or a stationary trench (upside-down triangles), and models with changing SP and  
 361 UP ages with rollback (circles) or a stationary trench (squares). For values of the crustal viscosity and  
 362 ages of plates see figure 8.

363

364 In our numerical experiments with varying plate age, the amplitude and period of the oscillations in  
 365 plate velocity depend on the average subduction velocity (Figure 7, 8a-f). Models with a younger  
 366 overriding plate and therefore a shorter subduction interface, have higher average subduction  
 367 velocities within the 40 Ma long time-period with steady-state, quasi-periodic buckling (Figure 8 a,b).  
 368 These velocities correlate directly to larger amplitudes (2-9 cm/a) in oscillations in the cases with  
 369 rollback (Figure 8e). The cases with a stationary trench show that the amplitude of  $V_{SP}$  oscillations is  
 370 predominantly determined by subducting plate age while the effect of the overriding plate age is  
 371 limited.  $V_{SP}$  amplitudes vary between 1-3 cm/a (Figure 8f). Hence, faster-subducting plates have  
 372 higher velocity amplitudes and lower periods of oscillation, and analogous to our reference models,  
 373 this trend is most profound in models that allow rollback, in which the amplitudes are 2-3 times  
 374 larger than in models with a mantle-stationary trench (Figure 7).

375 The models with a varying constant crustal viscosity show the same trend: higher average  
 376  $V_{SP}$ 's leads to larger velocity oscillation amplitudes (Figure 8 c,d) and smaller periods (Figure 8 g,h).  
 377 Models with a power law crustal viscosity have smaller variations in average  $V_{SP}$  between them than  
 378 those with a constant viscosity and consequently also smaller variations in oscillation amplitudes,  
 379 albeit with higher absolute amplitudes (Figure 8 c,d). This is the result of feedback mechanisms  
 380 between subducting plate velocity and the power law crustal viscosity (Pokorný et al., 2021), which  
 381 also keeps the period of  $V_{SP}$  oscillations constant (Figure 8 g,h).



382 **Figure 8 – Amplitude, Period and  $V_{SP}$  as function of plate age and crustal viscosity**  
 383  $V_{SP}$  as function of SP and OP ages for models with a moving trench (A) and a stationary trench (B).  
 384 Amplitude of the oscillating  $V_{SP}$  as function of the average  $V_{SP}$  for crustal viscosities:  $5e19$ ,  $1e20$ ,  $5e20$   
 385 (closed triangles) and three power law crustal viscosities (open triangles) in models with a moving  
 386 trench (C) and a stationary trench (D). Amplitude of the oscillating  $V_{SP}$  as function of SP and OP plate  
 387 ages for models with a moving trench (E) and a stationary trench (F). Period of the oscillating  $V_{SP}$  as  
 388 function of the average  $V_{SP}$  for a varying crustal viscosity in models with a moving trench (G) and a  
 389 stationary trench (H).  
 390  
 391

#### 392 4. Discussion

393 Slabs that subduct with plate motions exceeding the average lower mantle sinking rate of 1-  
 394 1.5 cm/a (Van der Meer et al., 2018) inevitably require that slabs shorten and thicken.  
 395 Interpretations of geophysical observations and subduction models (cited above), including our own,  
 396 show that this occurs through buckling of the slab in the MTZ (Figure 3). During slab buckling, the  
 397 slab dip in the top ~300 km alternates between steep (vertical or overturned) and inclined, and our



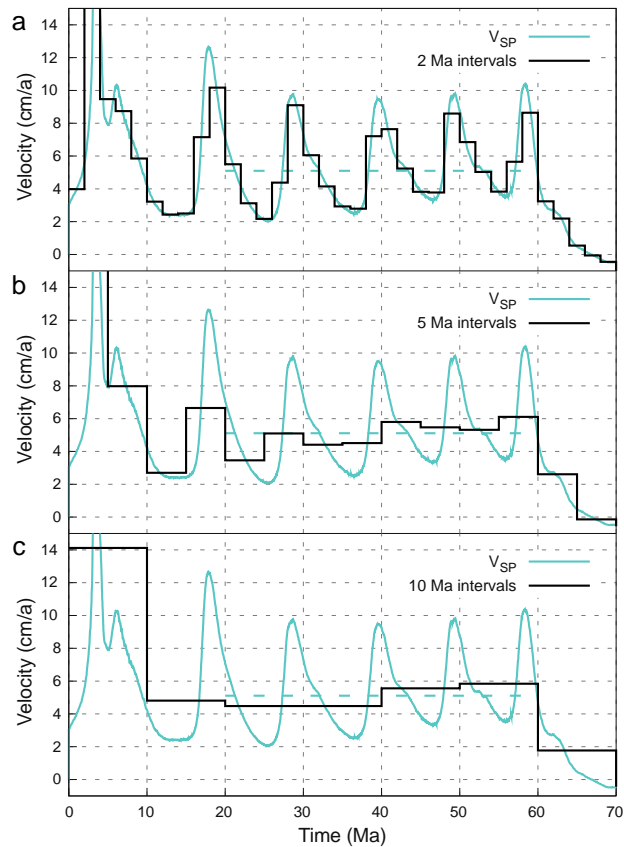
398 results illustrate that this induces alternating phases of slab rollback and stagnation (or advance), as  
399 well as motion of the trench and upper plate (Figure 5a). Our results reveal that these alternating  
400 phases of forward and backward buckling induce variations in subduction rate and subducting plate  
401 motion.

402 High subduction rates occur in our experiments when the slab buckles backward, towards  
403 the downgoing plate and adjacent to a previous slab fold. For backward buckling, the  
404 accommodation space in the MTZ in which the buckling slab can sink is available as opposed to  
405 forward buckling, in which case the lower part of the MTZ is still occupied by previously buckled slab  
406 (Figure 4a). As the 410 km phase transition enhances the negative buoyancy of slabs and thus  
407 enhances slab pull (Čížková & Bina, 2013) the accommodation in the MTZ for backward buckling  
408 allows the slab to force a short (in our reference model < 3 Ma) pulse of high  $V_{SP}$ , and roll-back.  
409 During roll-back, the slab steepens to a vertical orientation accompanied by limited motion of the  
410 trench (Figure 4b), or even trench advance if the upper plate rheology would allow it. Once the slab  
411 overturns the next forward buckle initiates, during which time MTZ accommodation space  
412 decreases. A forward buckle is associated with trench retreat and slab advance in the MTZ,  
413 seemingly rotating over a pivot point in the upper mantle (Figure 4a). As a result,  $V_{SP}$  decreases  
414 during a forward buckling slab while  $V_{UP}$  increases. As the slab flattens during this forward buckle it  
415 creates accommodation space for the next backward buckle and associated acceleration (Figure 4b).

416  $V_{SP}$  variations in models with a forced stationary trench are smaller because the slab has less  
417 variation in the amount of accommodation space in the MTZ. Trench-stationary subduction causes  
418 the slab buckling in a vertical column (Figure 3i-n). Basically, the rate and amplitude of plate motion  
419 oscillation primarily depends on the average  $V_{SP}$ : the higher, the bigger the space accommodation  
420 problem for slab folds in the MTZ. Our experiments with a moving trench and an average  $V_{SP}$  of 6  
421 cm/a, i.e., the global average plate velocity (Van Der Meer et al., 2014), reveal rapid oscillations (< 10  
422 Ma periods) with large  $V_{SP}$  fluctuations (3-13 cm/a) (Figure 6).

423 The rapid subducting plate motion oscillations that we find in our experiments have similar  
424 periods to those recently observed in the high-resolution (0.5-1 Ma) reconstruction of marine  
425 magnetic anomalies of the Indian Ocean (DeMets & Merkouriev, 2021). Previous plate  
426 reconstructions using stage rotations based on larger stage intervals of 5-10 Ma (Figure 2) (Müller et  
427 al., 2019; van Hinsbergen et al., 2011) smoothed out such rapid plate motion changes (Espinoza &  
428 Iaffaldano, 2023; White & Lister, 2012). We illustrate this by sampling  $V_{SP}$  in our reference  
429 experiment with a mobile upper plate: when we sample on a 1-2 Ma resolution, similar to DeMets &  
430 Merkouriev (2021) we resolve rapid (< 5 Ma) oscillations in plate motion caused by slab buckling  
431 (Figure 9a). However, sampling our  $V_{SP}$  curves at larger, typically used intervals of 5 or 10 Ma

432 generates the smooth plate motion history that is widely inferred from plate reconstructions (Figure  
433 9 b,c).



434  
435 **Figure 9 – Sampling intervals for subducting plate velocity**

436 Horizontal subducting plate motion for the reference model with rollback and stage velocities if  
437 sampled at 2, 5 or 10 Ma intervals.

438  
439 The average  $V_{SP}$  as well as the amplitudes of the plate motion oscillations for the case of  
440 India are higher than in our experiments. These differences are likely at least in part explained by the  
441 simplicity of our model: the absolute plate motion rate of India may have been much higher than we  
442 obtained in our experiments because the Indian plate may have been lubricated at the base by a  
443 mantle plume (Kumar et al., 2007; van Hinsbergen et al., 2011), or the subduction interface may  
444 have been heavily lubricated by sediments (Behr & Becker, 2018). The buckling behaviour may have  
445 differed because Indian subduction rates were not uniform along-strike, but increased eastward (van  
446 Hinsbergen et al., 2011) and the lithosphere in the MTZ during the 55-50 Ma ago interval during  
447 which the oscillations were reconstructed may have been of continental origin (van Hinsbergen et  
448 al., 2019). This could have influenced the effects of the MTZ on slab pull, the rate of slab transfer  
449 into the lower mantle, and the amount of accommodation space in the MTZ, which would all  
450 influence the oscillation  $V_{SP}$  amplitude and period in our experiments.

451 An additional difference with our simple experiments is that subduction of the Indian plate  
452 occurred at a trench that was not retreating, as in our experiments, but instead slowly moving

453 northwards, i.e. advancing (van Hinsbergen et al., 2019). In our experiments, subduction at a mantle-  
454 stationary trench occurs with lower amplitude oscillations than those reconstructed by DeMets &  
455 Merkouriev (2021). However, the Indian slab may have advanced below the upper plate and  
456 retreated without significantly affecting trench motion as in our experiments. Slab buckling  
457 combined with trench advance could create an opposite regime as in our experiments, with  
458 acceleration during forward buckles and vice versa. Trench motion can even alternate between  
459 retreat and advance (Stegman et al., 2010). This could explain the ~1000 km wide north to south  
460 tomographic anomaly widely interpreted as the Indian slab (Qayyum et al., 2022). We foresee that  
461 these processes may produce variations in MTZ accommodation space even when the trench is  
462 nearly stationary. Modelling such additional complexities is beyond the scope of our investigation:  
463 with the even higher subduction rates for India than we reproduced in our experiments, the space  
464 problem in the MTZ must have been even larger than in our experiments, and we therefore consider  
465 buckling a plausible candidate to explain the reconstructed oscillations.

466 In our slab-pull-driven subduction models with a freely moving upper plate we also observe  
467 oscillating motion of the trench and upper plate. In our simple experiments, the rigid upper plate is  
468 not able to deform, and it thus moves along with the trench where naturally this would lead to  
469 changes in stress state, reflected by episodic extensional or contractional upper plate deformation  
470 (Billen & Arredondo, 2018; Boutoux et al., 2021; Capitanio et al., 2010; Cerpa et al., 2018; Dasgupta  
471 et al., 2021; Lee & King, 2011; Pons et al., 2022; Van Hinsbergen & Schouten, 2021). Such variations  
472 may be of interest to the understanding of fluid and magmatic processes affecting the upper plate.  
473 For instance, episodic magmatic ponding alternating with migration and flare ups (Chapman et al.,  
474 2021), and episodic mineralization (Chelle-Michou et al., 2015) and associated pulses in the  
475 formation of ore deposits (Wilson et al., 2020) may be the result of such stress state oscillations.  
476 Therefore, for subduction zones where slab buckling leads to oscillating trench motion and upper  
477 plate deformation, enhanced resolution in marine magnetic anomalies and accompanying  
478 reconstructions could lead to a better predictive power in the timing of these magmatic and ore-  
479 genesis related upper plate processes. In the Andes, alternations on a timescale of ~10 Ma between  
480 shortening and trench retreat were recently postulated to result from slab buckling (Pons et al.,  
481 2022). For Tibet, the only high-resolution deformation records in the relevant time interval of 60-50  
482 Ma are from the Qiangtang terrane of northern Tibet, far from the trench (Li, van Hinsbergen,  
483 Najman, et al., 2020; Li, van Hinsbergen, Shen, et al., 2020), which on a first order appear to record  
484 shortening pulses that coincide with the oscillations (DeMets & Merkouriev, 2021). More high-  
485 resolution work, for instance in the Xigaze forearc basin, could reveal whether the upper plate may  
486 also have recorded short periods of extension.

487            Would all subducting plates then show these oscillating plate motions? Higher-resolution  
488 tectonic reconstructions could provide the answer, but we see several reasons why not all ridges  
489 that border subducting plates may record such oscillations similarly. The process of buckling at long  
490 subduction zones might not occur synchronously along the entire trench. Such a process may explain  
491 the oscillating azimuth of India-Asia convergence during the oscillations documented DeMets &  
492 Merkouriev (2021). In addition, subduction rate may vary gradually along-strike of a trench (e.g., the  
493 west Pacific subduction zones from New Zealand to Kamchatka), and rapidly across triple junctions  
494 (e.g., Vaes et al., 2019; van de Lagemaat et al., 2018). Plates like the modern Pacific plate would be  
495 less susceptible to the effect of slab buckling in the MTZ, even if the oscillations in a 2D system likely  
496 occur. We foresee that oscillations in plate motion are best visible for plates where subduction zones  
497 are oriented sub-parallel to spreading ridges and sub-perpendicular to the plate motion direction.  
498 Possible candidates for the Cenozoic besides the Indian plate are the Nazca plate (Pons et al., 2022),  
499 the Juan de Fuca plate, the Cocos plate, or the Aluk plate (van de Lagemaat et al., 2023) and for  
500 earlier times perhaps the Farallon or Kula plates. We consider these targets for high-resolution  
501 magnetic anomaly reconstruction to further test the possibilities of slab buckling and the  
502 opportunities it may apply to understand mantle and lithosphere dynamics and magmatic and  
503 economic geology.  
504 Finally, our models show that the rapid oscillations shown by DeMets & Merkouriev (2021) may well  
505 be explained by buckling of the subducting slab that results from the space problem caused by the  
506 much lower sinking rates of slabs in the lower mantle. This implies that plate motions that exceed  
507 lower mantle slab sinking rates, so larger than 1-1.5 cm/a (Butterworth et al., 2014; Van Der Meer et  
508 al., 2010; Van der Meer et al., 2018), are resisted from the transition zone downwards. In other  
509 words, typical plate motions must be primarily driven in the top few hundred kilometers of the  
510 mantle. The 410 km phase transition still enhances slab pull, but at the 660 discontinuity the slab  
511 encounters resistance and thickens. In addition, the top 100 km of the Earth also resists plate motion  
512 due to friction on the subduction interface or drag resistance from the underlying mantle, therefore  
513 plate tectonics must primarily be driven between depths of ~100 and 500 km, or only 6-7% of the  
514 Earth's radius. This is a remarkably small niche that on Earth apparently has the right conditions for  
515 plate tectonics. We foresee that understanding the dynamics of this narrow zone throughout Earth's  
516 history holds the key to understand the uniqueness of our planet to start and sustain plate tectonics.

## 517 Conclusions

518 Buckling of a slab in the mantle transition zone may explain the rapid oscillations in subducting plate  
519 motion recently shown in high-resolution reconstructions. The amplitude and period of these

520 oscillations depend on the average subduction speed and accommodation space in the mantle  
521 transition zone. Furthermore, it may also cause episodic migration of a trench and rapid deformation  
522 pulses of the upper plate. This mechanism reveals that slab pull might only be an effective plate  
523 motion driver in the top few hundred kilometers of the upper mantle.

524

## 525 References

- 526 Androvičová, A., Čížková, H., & van den Berg, A. (2013). The effects of rheological decoupling  
527 on slab deformation in the Earth's upper mantle. *Studia Geophysica et Geodaetica*,  
528 57, 460-481.
- 529
- 530 Běhouňková, M., & Čížková, H. (2008). Long-wavelength character of subducted slabs in the  
531 lower mantle. *Earth and Planetary Science Letters*, 275(1-2), 43-53.
- 532
- 533 Behr, W. M., & Becker, T. W. (2018). Sediment control on subduction plate speeds. *Earth*  
534 *and Planetary Science Letters*, 502, 166-173.
- 535
- 536 Behr, W. M., Holt, A. F., Becker, T. W., & Faccenna, C. (2022). The effects of plate interface  
537 rheology on subduction kinematics and dynamics. *Geophysical Journal International*,  
538 230(2), 796-812.
- 539
- 540 Bercovici, D., Schubert, G., & Ricard, Y. (2015). Abrupt tectonics and rapid slab detachment  
541 with grain damage. *Proceedings of the National Academy of Sciences*, 112(5), 1287-  
542 1291.
- 543
- 544 Billen, M. I., & Arredondo, K. M. (2018). Decoupling of plate-asthenosphere motion caused  
545 by non-linear viscosity during slab folding in the transition zone. *Physics of the Earth*  
546 *and planetary interiors*, 281, 17-30.
- 547
- 548 Bina, C. R., & Helffrich, G. (1994). Phase transition Clapeyron slopes and transition zone  
549 seismic discontinuity topography. *Journal of Geophysical Research: Solid Earth*,  
550 99(B8), 15853-15860.
- 551
- 552 Boutoux, A., Briaud, A., Faccenna, C., Ballato, P., Rossetti, F., & Blanc, E. (2021). Slab folding  
553 and surface deformation of the Iran mobile belt. *Tectonics*, 40(6), e2020TC006300.
- 554
- 555 Butterworth, N., Talsma, A., Müller, R., Seton, M., Bunge, H.-P., Schuberth, B., Shephard, G.,  
556 & Heine, C. (2014). Geological, tomographic, kinematic and geodynamic constraints  
557 on the dynamics of sinking slabs. *Journal of Geodynamics*, 73, 1-13.  
558 <https://doi.org/10.1016/j.jog.2013.10.006>
- 559
- 560 Capitanio, F., Faccenna, C., Zlotnik, S., & Stegman, D. (2011). Subduction dynamics and the  
561 origin of Andean orogeny and the Bolivian orocline. *Nature*, 480(7375), 83-86.
- 562

563 Capitano, F. A., Stegman, D. R., Moresi, L.-N., & Sharples, W. (2010). Upper plate controls  
564 on deep subduction, trench migrations and deformations at convergent margins.  
565 *Tectonophysics*, 483(1-2), 80-92.  
566

567 Cerpa, N. G., Guillaume, B., & Martinod, J. (2018). The interplay between overriding plate  
568 kinematics, slab dip and tectonics. *Geophysical Journal International*, 215(3), 1789-  
569 1802.  
570

571 Chapman, J. B., Shields, J. E., Ducea, M. N., Paterson, S. R., Attia, S., & Ardill, K. E. (2021). The  
572 causes of continental arc flare ups and drivers of episodic magmatic activity in  
573 Cordilleran orogenic systems. *Lithos*, 398, 106307.  
574

575 Chelle-Michou, C., Chiaradia, M., Selby, D., Ovtcharova, M., & Spikings, R. A. (2015). High-  
576 resolution geochronology of the Corocohuayco porphyry-skarn deposit, Peru: A  
577 rapid product of the Incaic orogeny. *Economic Geology*, 110(2), 423-443.  
578

579 Chen, Y.-W., Wu, J., & Suppe, J. (2019). Southward propagation of Nazca subduction along  
580 the Andes. *Nature*, 565(7740), 441-447.  
581

582 Christensen, U. R., & Yuen, D. A. (1985). Layered convection induced by phase transitions.  
583 *Journal of Geophysical Research: Solid Earth*, 90(B12), 10291-10300.  
584

585 Čížková, H., & Bina, C. R. (2013). Effects of mantle and subduction-interface rheologies on  
586 slab stagnation and trench rollback. *Earth and Planetary Science Letters*, 379, 95-103.  
587

588 Čížková, H., & Bina, C. R. (2019). Linked influences on slab stagnation: Interplay between  
589 lower mantle viscosity structure, phase transitions, and plate coupling. *Earth and  
590 Planetary Science Letters*, 509, 88-99.  
591

592 Čížková, H., van den Berg, A. P., Spakman, W., & Matyska, C. (2012). The viscosity of Earth's  
593 lower mantle inferred from sinking speed of subducted lithosphere. *Physics of the  
594 Earth and planetary interiors*, 200, 56-62.  
595 <https://doi.org/10.1016/j.pepi.2012.02.010>  
596

597 Čížková, H., van Hunen, J., & van den Berg, A. (2007). Stress distribution within subducting  
598 slabs and their deformation in the transition zone. *Physics of the Earth and planetary  
599 interiors*, 161(3-4), 202-214.  
600

601 Čížková, H., van Hunen, J., van den Berg, A. P., & Vlaar, N. J. (2002). The influence of  
602 rheological weakening and yield stress on the interaction of slabs with the 670 km  
603 discontinuity. *Earth and Planetary Science Letters*, 199(3-4), 447-457.  
604

605 Coltice, N., Husson, L., Faccenna, C., & Arnould, M. (2019). What drives tectonic plates?  
606 *Science advances*, 5(10), eaax4295.  
607

608 Dasgupta, R., Mandal, N., & Lee, C. (2021). Controls of subducting slab dip and age on the  
609 extensional versus compressional deformation in the overriding plate.  
610 *Tectonophysics*, 801, 228716.  
611

612 DeMets, C., & Merkouriev, S. (2021). Detailed reconstructions of India–Somalia Plate  
613 motion, 60 Ma to present: implications for Somalia Plate absolute motion and India–  
614 Eurasia Plate motion. *Geophysical Journal International*, 227(3), 1730-1767.  
615

616 Doubrovine, P. V., Steinberger, B., & Torsvik, T. H. (2012). Absolute plate motions in a  
617 reference frame defined by moving hot spots in the Pacific, Atlantic, and Indian  
618 oceans. *Journal of Geophysical Research: Solid Earth*, 117(B9).  
619

620 Espinoza, V., & Iaffaldano, G. (2023). Rapid absolute plate motion changes inferred from  
621 high-resolution relative spreading reconstructions: A case study focusing on the  
622 South America plate and its Atlantic/Pacific neighbors. *Earth and Planetary Science  
623 Letters*, 604, 118009.  
624

625 Forsyth, D., & Uyeda, S. (1975). On the relative importance of the driving forces of plate  
626 motion. *Geophysical Journal International*, 43(1), 163-200.  
627

628 Garel, F., Goes, S., Davies, D., Davies, J. H., Kramer, S. C., & Wilson, C. R. (2014). Interaction  
629 of subducted slabs with the mantle transition-zone: A regime diagram from 2-D  
630 thermo-mechanical models with a mobile trench and an overriding plate.  
631 *Geochemistry, Geophysics, Geosystems*, 15(5), 1739-1765.  
632

633 Goes, S., Agrusta, R., van Hunen, J., & Garel, F. (2017). Subduction-transition zone  
634 interaction: A review. *Geosphere*, 13(3), 644-664.  
635

636 Goes, S., Capitanio, F., Morra, G., Seton, M., & Giardini, D. (2011). Signatures of downgoing  
637 plate-buoyancy driven subduction in Cenozoic plate motions. *Physics of the Earth  
638 and planetary interiors*, 184(1-2), 1-13.  
639

640 Gürer, D., Granot, R., & van Hinsbergen, D. J. (2022). Plate tectonic chain reaction revealed  
641 by noise in the Cretaceous quiet zone. *Nature Geoscience*, 15(3), 233-239.  
642

643 Hansen, U., Yuen, D., Kroening, S., & Larsen, T. (1993). Dynamical consequences of depth-  
644 dependent thermal expansivity and viscosity on mantle circulations and thermal  
645 structure. *Physics of the Earth and planetary interiors*, 77(3-4), 205-223.  
646

647 Hirth, G., & Kohlstedt, D. (2003). Rheology of the upper mantle and the mantle wedge: A  
648 view from the experimentalists. *Geophysical monograph-american geophysical  
649 union*, 138, 83-106.  
650

651 Holt, A. F., Becker, T., & Buffett, B. (2015). Trench migration and overriding plate stress in  
652 dynamic subduction models. *Geophysical Journal International*, 201(1), 172-192.  
653

654 Hu, J., Gurnis, M., Rudi, J., Stadler, G., & Müller, R. D. (2022). Dynamics of the abrupt change  
655 in Pacific Plate motion around 50 million years ago. *Nature Geoscience*, *15*(1), 74-78.  
656

657 Ita, J., & King, S. D. (1994). Sensitivity of convection with an endothermic phase change to  
658 the form of governing equations, initial conditions, boundary conditions, and  
659 equation of state. *Journal of Geophysical Research: Solid Earth*, *99*(B8), 15919-15938.  
660

661 Karato, S.-i. (2008). Deformation of earth materials. *An introduction to the rheology of Solid  
662 Earth*, 463.  
663

664 Karato, S.-i., Zhang, S., & Wenk, H.-R. (1995). Superplasticity in Earth's lower mantle:  
665 evidence from seismic anisotropy and rock physics. *Science*, *270*(5235), 458-461.  
666

667 Katsura, T., Shatskiy, A., Manthilake, M. G. M., Zhai, S., Fukui, H., Yamazaki, D., Matsuzaki, T.,  
668 Yoneda, A., Ito, E., & Kuwata, A. (2009). Thermal expansion of forsterite at high  
669 pressures determined by in situ X-ray diffraction: The adiabatic geotherm in the  
670 upper mantle. *Physics of the Earth and planetary interiors*, *174*(1-4), 86-92.  
671

672 Katsura, T., Yamada, H., Nishikawa, O., Song, M., Kubo, A., Shinmei, T., Yokoshi, S., Aizawa,  
673 Y., Yoshino, T., & Walter, M. J. (2004). Olivine-wadsleyite transition in the system  
674 (Mg, Fe)  $2\text{SiO}_4$ . *Journal of Geophysical Research: Solid Earth*, *109*(B2).  
675

676 Knesel, K. M., Cohen, B. E., Vasconcelos, P. M., & Thiede, D. S. (2008). Rapid change in drift  
677 of the Australian plate records collision with Ontong Java plateau. *Nature*,  
678 *454*(7205), 754-757.  
679

680 Kumar, P., Yuan, X., Kumar, M. R., Kind, R., Li, X., & Chadha, R. (2007). The rapid drift of the  
681 Indian tectonic plate. *Nature*, *449*(7164), 894-897.  
682

683 Lee, C., & King, S. D. (2011). Dynamic buckling of subducting slabs reconciles geological and  
684 geophysical observations. *Earth and Planetary Science Letters*, *312*(3-4), 360-370.  
685

686 Li, S., van Hinsbergen, D. J., Najman, Y., Liu-Zeng, J., Deng, C., & Zhu, R. (2020). Does pulsed  
687 Tibetan deformation correlate with Indian plate motion changes? *Earth and  
688 Planetary Science Letters*, *536*, 116144.  
689

690 Li, S., van Hinsbergen, D. J., Shen, Z., Najman, Y., Deng, C., & Zhu, R. (2020). Anisotropy of  
691 magnetic susceptibility (AMS) analysis of the Gonjo Basin as an independent  
692 constraint to date Tibetan shortening pulses. *Geophysical Research Letters*, *47*(8),  
693 e2020GL087531.  
694

695 Lithgow-Bertelloni, C., & Richards, M. A. (1998). The dynamics of Cenozoic and Mesozoic  
696 plate motions. *Reviews of Geophysics*, *36*(1), 27-78.  
697

698 Morishima, H., Kato, T., Suto, M., Ohtani, E., Urakawa, S., Utsumi, W., Shimomura, O., &  
699 Kikegawa, T. (1994). The phase boundary between  $\alpha$ - and  $\beta$ - $\text{Mg}_2\text{SiO}_4$  determined by  
700 in situ X-ray observation. *Science*, *265*(5176), 1202-1203.



701  
702 Müller, R. D., Flament, N., Cannon, J., Tetley, M. G., Williams, S. E., Cao, X., Bodur, Ö. F.,  
703 Zahirovic, S., & Meredith, A. (2022). A tectonic-rules-based mantle reference frame  
704 since 1 billion years ago—implications for supercontinent cycles and plate–mantle  
705 system evolution. *Solid Earth*, *13*(7), 1127-1159.  
706  
707 Müller, R. D., Zahirovic, S., Williams, S. E., Cannon, J., Seton, M., Bower, D. J., Tetley, M. G.,  
708 Heine, C., Le Breton, E., & Liu, S. (2019). A global plate model including lithospheric  
709 deformation along major rifts and orogens since the Triassic. *Tectonics*, *38*(6), 1884-  
710 1907.  
711  
712 Parsons, A. J., Sigloch, K., & Hosseini, K. (2021). Australian Plate Subduction is Responsible  
713 for Northward Motion of the India-Asia Collision Zone and ~ 1,000 km Lateral  
714 Migration of the Indian Slab. *Geophysical Research Letters*, *48*(18), e2021GL094904.  
715 <https://doi.org/10.1029/2021GL094904>  
716  
717 Patriat, P., & Achache, J. (1984). India–Eurasia collision chronology has implications for  
718 crustal shortening and driving mechanism of plates. *Nature*, *311*(5987), 615-621.  
719  
720 Pokorný, J., Čížková, H., & van den Berg, A. (2021). Feedbacks between subduction dynamics  
721 and slab deformation: Combined effects of nonlinear rheology of a weak decoupling  
722 layer and phase transitions. *Physics of the Earth and planetary interiors*, *313*, 106679.  
723  
724 Pons, M., Sobolev, S. V., Liu, S., & Neuharth, D. (2022). Hindered trench migration due to  
725 slab steepening controls the formation of the Central Andes. *Journal of Geophysical*  
726 *Research: Solid Earth*, e2022JB025229.  
727  
728 Qayyum, A., Lom, N., Advokaat, E. L., Spakman, W., Van Der Meer, D. G., & van Hinsbergen,  
729 D. J. (2022). Subduction and Slab Detachment Under Moving Trenches During  
730 Ongoing India-Asia Convergence. *Geochemistry, Geophysics, Geosystems*, *23*(11),  
731 e2022GC010336.  
732  
733 Ranalli, G. (1995). *Rheology of the Earth*. Springer Science & Business Media.  
734  
735 Replumaz, A., Karason, H., van der Hilst, R. D., Besse, J., & Tapponnier, P. (2004). 4-D  
736 evolution of SE Asia’s mantle from geological reconstructions and seismic  
737 tomography. *Earth and Planetary Science Letters*, *221*(1-4), 103-115.  
738  
739 Ribe, N. M., Stutzmann, E., Ren, Y., & Van Der Hilst, R. (2007). Buckling instabilities of  
740 subducted lithosphere beneath the transition zone. *Earth and Planetary Science*  
741 *Letters*, *254*(1-2), 173-179.  
742  
743 Schellart, W. P. (2005). Influence of the subducting plate velocity on the geometry of the  
744 slab and migration of the subduction hinge. *Earth and Planetary Science Letters*,  
745 *231*(3-4), 197-219.  
746

747 Sdrolias, M., & Müller, R. D. (2006). Controls on back-arc basin formation. *Geochemistry,*  
748 *Geophysics, Geosystems, 7*(4).  
749

750 Segal, A., & Praagman, N. (2005). The sepran fem package. *Tech. Report, Ingenieursbureau*  
751 *Sepra, Netherlands.*  
752

753 Sigloch, K., & Mihalynuk, M. G. (2013). Intra-oceanic subduction shaped the assembly of  
754 Cordilleran North America. *Nature, 496*(7443), 50-56.  
755

756 Spakman, W., Chertova, M. V., van den Berg, A., & van Hinsbergen, D. J. (2018). Puzzling  
757 features of western Mediterranean tectonics explained by slab dragging. *Nature*  
758 *Geoscience, 11*(3), 211-216.  
759

760 Stegman, D. R., Farrington, R., Capitanio, F. A., & Schellart, W. P. (2010). A regime diagram  
761 for subduction styles from 3-D numerical models of free subduction. *Tectonophysics,*  
762 *483*(1-2), 29-45.  
763

764 Steinbach, V., & Yuen, D. A. (1995). The effects of temperature-dependent viscosity on  
765 mantle convection with the two major phase transitions. *Physics of the Earth and*  
766 *planetary interiors, 90*(1-2), 13-36.  
767

768 Su, C., Liu, Y., Fan, D., Song, W., Jiang, J., Sun, Z., & Yang, G. (2022). Thermodynamic  
769 Properties of Fe-Bearing Wadsleyite and Determination of the Olivine-Wadsleyite  
770 Phase Transition Boundary in (Mg, Fe) 2SiO<sub>4</sub> System. *Frontiers in Earth Science, 10,*  
771 *879678.*  
772

773 Torsvik, T. H., Müller, R. D., Van der Voo, R., Steinberger, B., & Gaina, C. (2008). Global plate  
774 motion frames: toward a unified model. *Reviews of Geophysics, 46*(3).  
775

776 Vaes, B., Van Hinsbergen, D. J., & Boschman, L. M. (2019). Reconstruction of subduction and  
777 back-arc spreading in the NW Pacific and Aleutian Basin: Clues to causes of  
778 Cretaceous and Eocene plate reorganizations. *Tectonics, 38*(4), 1367-1413.  
779

780 van de Lagemaat, S. H., Kamp, P. J., Boschman, L. M., & Van Hinsbergen, D. J. (2023).  
781 Reconciling the Cretaceous breakup and demise of the Phoenix Plate with East  
782 Gondwana orogenesis in New Zealand. *Earth-Science Reviews, 104276.*  
783

784 van de Lagemaat, S. H., Van Hinsbergen, D. J., Boschman, L. M., Kamp, P. J., & Spakman, W.  
785 (2018). Southwest Pacific absolute plate kinematic reconstruction reveals major  
786 Cenozoic Tonga-Kermadec slab dragging. *Tectonics, 37*(8), 2647-2674.  
787

788 van den Berg, A., Segal, G., & Yuen, D. A. (2015). SEPRAN: A versatile finite-element package  
789 for a wide variety of problems in geosciences. *Journal of Earth Science, 26,* 89-95.  
790

791 van den Berg, A. P., van Keken, P. E., & Yuen, D. A. (1993). The effects of a composite non-  
792 Newtonian and Newtonian rheology on mantle convection. *Geophysical Journal*  
793 *International, 115*(1), 62-78.

794  
795 Van Der Meer, D. G., Spakman, W., Van Hinsbergen, D. J., Amaru, M. L., & Torsvik, T. H.  
796 (2010). Towards absolute plate motions constrained by lower-mantle slab remnants.  
797 *Nature Geoscience*, 3(1), 36-40. <https://doi.org/10.1038/ngeo708>  
798  
799 Van der Meer, D. G., Van Hinsbergen, D. J., & Spakman, W. (2018). Atlas of the underworld:  
800 Slab remnants in the mantle, their sinking history, and a new outlook on lower  
801 mantle viscosity. *Tectonophysics*, 723, 309-448.  
802 <https://doi.org/10.1016/j.tecto.2017.10.004>  
803  
804 Van Der Meer, D. G., Zeebe, R. E., van Hinsbergen, D. J., Sluijs, A., Spakman, W., & Torsvik, T.  
805 H. (2014). Plate tectonic controls on atmospheric CO2 levels since the Triassic.  
806 *Proceedings of the National Academy of Sciences*, 111(12), 4380-4385.  
807 <https://doi.org/10.1073/pnas.1315657111>  
808  
809 Van der Voo, R., Spakman, W., & Bijwaard, H. (1999). Tethyan subducted slabs under India.  
810 *Earth and Planetary Science Letters*, 171(1), 7-20. [https://doi.org/10.1016/S0012-](https://doi.org/10.1016/S0012-821X(99)00131-4)  
811 [821X\(99\)00131-4](https://doi.org/10.1016/S0012-821X(99)00131-4)  
812  
813 van Hinsbergen, D. J., Lippert, P. C., Li, S., Huang, W., Advokaat, E. L., & Spakman, W. (2019).  
814 Reconstructing Greater India: Paleogeographic, kinematic, and geodynamic  
815 perspectives. *Tectonophysics*, 760, 69-94.  
816  
817 Van Hinsbergen, D. J., & Schouten, T. L. (2021). Deciphering paleogeography from orogenic  
818 architecture: constructing orogens in a future supercontinent as thought  
819 experiment. *American Journal of Science*, 321(6), 955-1031.  
820  
821 van Hinsbergen, D. J., Steinberger, B., Doubrovine, P. V., & Gassmüller, R. (2011).  
822 Acceleration and deceleration of India-Asia convergence since the Cretaceous: Roles  
823 of mantle plumes and continental collision. *Journal of Geophysical Research: Solid*  
824 *Earth*, 116(B6).  
825  
826 van Hinsbergen, D. J., Steinberger, B., Guilmette, C., Maffione, M., Gürer, D., Peters, K.,  
827 Plunder, A., McPhee, P. J., Gaina, C., & Advokaat, E. L. (2021). A record of plume-  
828 induced plate rotation triggering subduction initiation. *Nature Geoscience*, 14(8),  
829 626-630.  
830  
831 White, L. T., & Lister, G. S. (2012). The collision of India with Asia. *Journal of Geodynamics*,  
832 56, 7-17.  
833  
834 Wilson, C. J., Moore, D. H., Vollgger, S. A., & Madeley, H. E. (2020). Structural evolution of  
835 the orogenic gold deposits in central Victoria, Australia: The role of regional stress  
836 change and the tectonic regime. *Ore Geology Reviews*, 120, 103390.  
837  
838 Wortel, R., & Cloetingh, S. (1981). On the origin of the Cocos-Nazca spreading center.  
839 *Geology*, 9(9), 425-430.  
840

841 Wu, J., Suppe, J., Lu, R., & Kanda, R. (2016). Philippine Sea and East Asian plate tectonics  
842 since 52 Ma constrained by new subducted slab reconstruction methods. *Journal of*  
843 *Geophysical Research: Solid Earth*, 121(6), 4670-4741.  
844  
845 Xue, K., Schellart, W. P., & Strak, V. (2022). Overriding plate deformation and topography  
846 during slab rollback and slab rollover: insights from subduction experiments.  
847 *Tectonics*, 41(2), e2021TC007089.  
848  
849 Zahirovic, S., Müller, R. D., Seton, M., & Flament, N. (2015). Tectonic speed limits from plate  
850 kinematic reconstructions. *Earth and Planetary Science Letters*, 418, 40-52.  
851 <https://doi.org/10.1016/j.epsl.2015.02.037>  
852

853 **Acknowledgements**

854 **Funding:**

855 Netherlands Organisation for Scientific Research, NWO Vici Grant 865.17.001 (EvdW, DJJvH)

856 Charles University Grant Agency, grant number 36121 (JP), grant SVV 260709 (JP, HC)

857 Czech Science Foundation, grant 23-06345S (JP, HC)

858 We thank Craig R. Bina for fruitful discussions.

859

860 **Open Research**

861 All modelling data that is used to produce the figures in this manuscript can be found on Zenodo:

862 10.5281/zenodo.10159525

863

864 **Author contributions**

865 Conceptualization: EvdW, JP, DJJvH

866 Methodology: EvdW, JP, HC, APvdB

867 Investigation: EvdW, JP

868 Visualization: EvdW, JP

869 Supervision: HC, DJJvH

870 Writing – original draft: EvdW, JP

871 Writing – review & editing: all authors

872

873 **Competing interests:**

874 Authors declare that they have no competing interests.

875

Table 1  
Model parameters

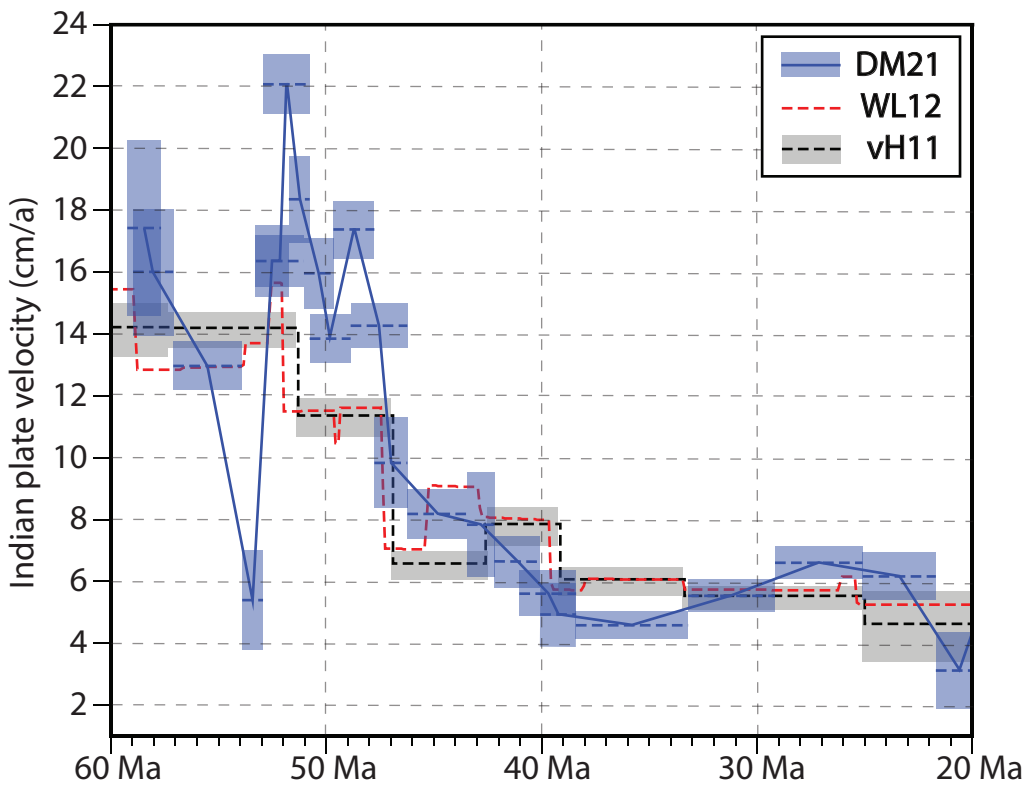
symbol	Meaning	Value	Units
Upper mantle and oceanic lithosphere rheology			
$A_{diff}$	Pre-exponential parameter of diffusion creep <sup>a</sup>	$1 \times 10^{-9}$	$Pa^{-1} s^{-1}$
$A_{dist}$	Pre-exponential parameter of dislocation creep <sup>a</sup>	$31.5 \times 10^{-18}$	$Pa^{-n} s^{-1}$
$E_{diff}$	Activation energy of diffusion creep <sup>a</sup>	$3.35 \times 10^5$	$J mol^{-1}$
$E_{dist}$	Activation energy of dislocation creep <sup>a</sup>	$4.8 \times 10^5$	$J mol^{-1}$
$V_{diff}$	Activation volume of diffusion creep <sup>a</sup>	$4.0 \times 10^{-6}$	$m^3 mol^{-1}$
$V_{dist}$	Activation volume of dislocation creep <sup>a</sup>	$11 \times 10^{-6}$	$m^3 mol^{-1}$
$\eta_{diff}$	Viscosity of diffusion creep	–	$Pa s$
$\eta_{dist}$	Viscosity of dislocation creep	–	$Pa s$
$\eta_y$	Power-law stress limiter viscosity	–	$Pa s$
$n$	dislocation creep exponent	3.5	–
$\dot{\epsilon}_y$	Reference strain rate	$1 \times 10^{-15}$	$s^{-1}$
$\sigma_y$	Stress limit	$2 - 5 \times 10^8$	$Pa$
$p$	Hydrostatic pressure	–	$Pa$
$n_y$	Stress limit exponent	10	–
$R$	Gas constant	8.314	$J K^{-1} mol^{-1}$
$T$	Temperature	–	K
$\dot{\epsilon}_{  }$	Second invariant of strainrate	–	$s^{-1}$
Lower mantle rheology			
$A_{diff}$	Pre-exponential parameter of diffusion creep	$1.3 \times 10^{-16}$	$Pa^{-1} s^{-1}$
$E_{diff}$	Activation energy of diffusion creep <sup>b</sup>	$2 \times 10^5$	$J mol^{-1}$
$V_{diff}$	Activation volume of diffusion creep <sup>b</sup>	$1.1 \times 10^{-6}$	$m^3 mol^{-1}$
Other model parameters			
$\eta_c$	Range of constant viscosity crust values	$5 \times 10^{19} - 5 \times 10^{20}$	$Pa s$
$\kappa$	Thermal diffusivity	$10^{-6}$	$m^2 s^{-1}$
$g$	Gravitational acceleration	9.8	$m^2 s^{-2}$
$\rho_0$	Reference density	3416	$kg m^{-3}$
$c_p$	Specific heat	1250	$J kg^{-1} K^{-1}$
$\alpha_0$	Surface thermal expansivity	$3 \times 10^{-5}$	$K^{-1}$
$\gamma_{410}$	Clapeyron slope of 410 km phase transition <sup>c</sup>	$3 \times 10^6$	$Pa K^{-1}$
$\gamma_{660}$	Clapeyron slope of 660 km phase transition <sup>c</sup>	$-1.5 \times 10^6$	$Pa K^{-1}$
$\delta_{\rho 410}$	Density contrast of 410 km phase transition <sup>d</sup>	273	$kg m^{-3}$
$\delta_{\rho 660}$	Density contrast of 660 km phase transition <sup>d</sup>	341	$kg m^{-3}$
Nonlinear crustal rheology			
$A_c$	Pre-exponential parameter of dislocation creep	$2.5 \times 10^{-17}$	$Pa^{-1} s^{-1}$
$E_c$	Activation energy of dislocation creep	$1.54 \times 10^5$	$J mol^{-1}$
$V_c$	Activation volume of dislocation creep	0	$m^3 mol^{-1}$
$n_c$	dislocation creep exponent	2.3	–
$\tau_c$	Cohesion	$0.25 - 1 \times 10^7$	$Pa$
$\mu_c$	Friction coefficient	0.025 – 0.1	–
$\sigma_y^c$	Stress limit in the crust	–	$Pa$

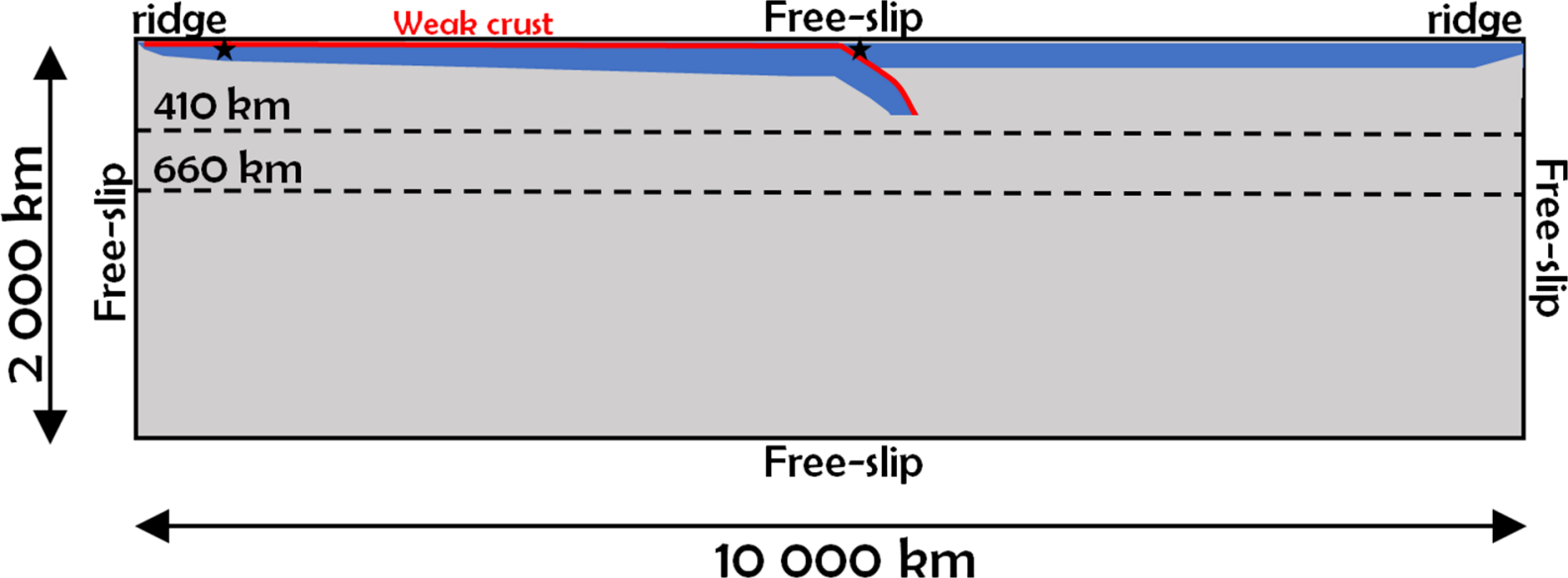
(a) Parameters of wet olivine based on Hirth and Kohlstedt (2003).

(b) Čížková et al. (2012).

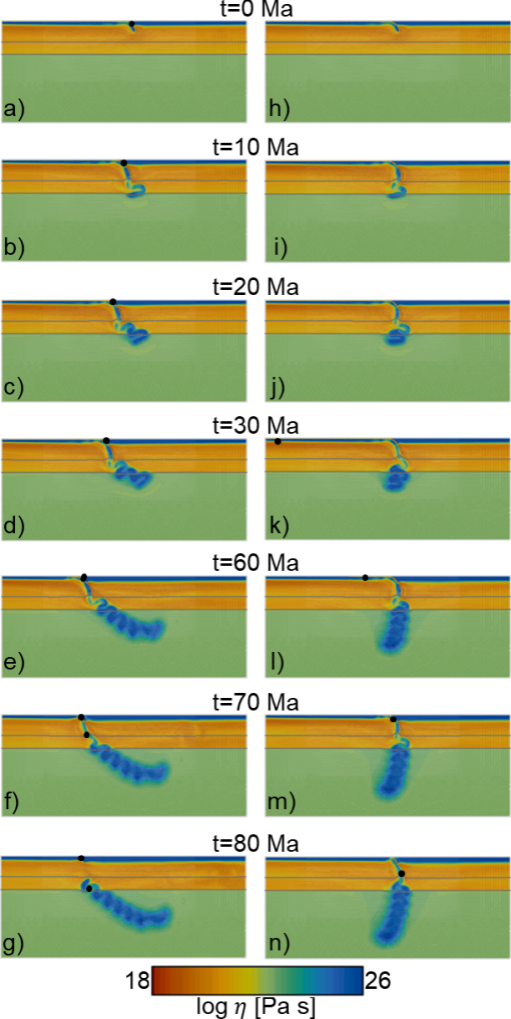
(c) Bina and Helffrich (1994).

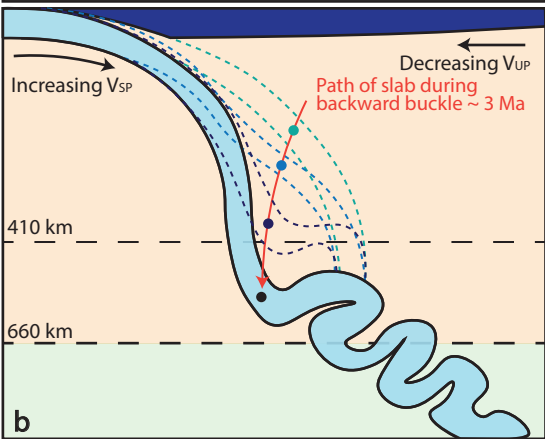
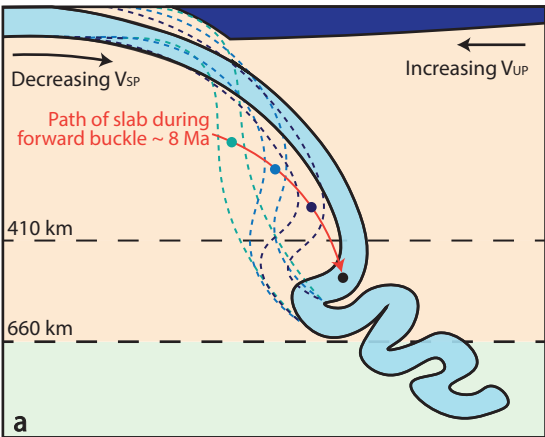
(d) Steinbach and Yuen (1995).

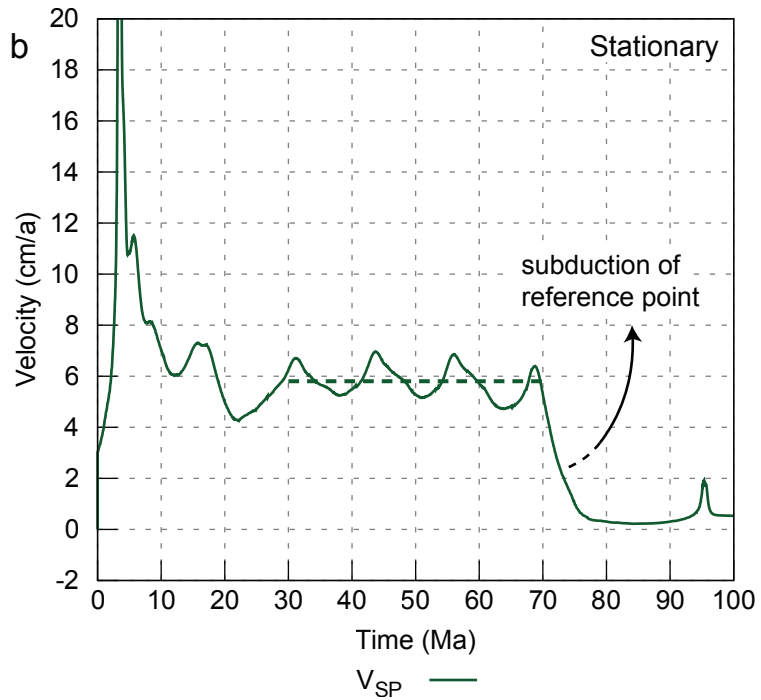
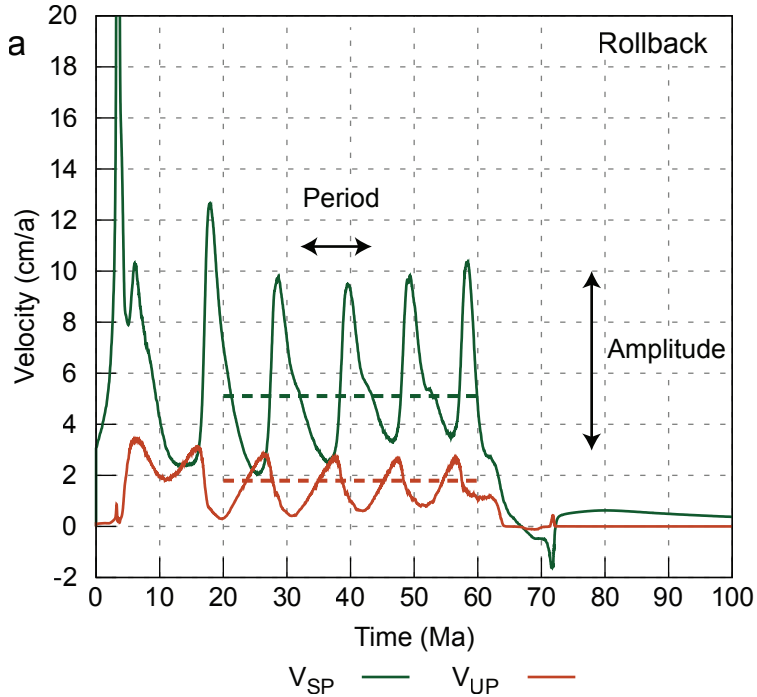


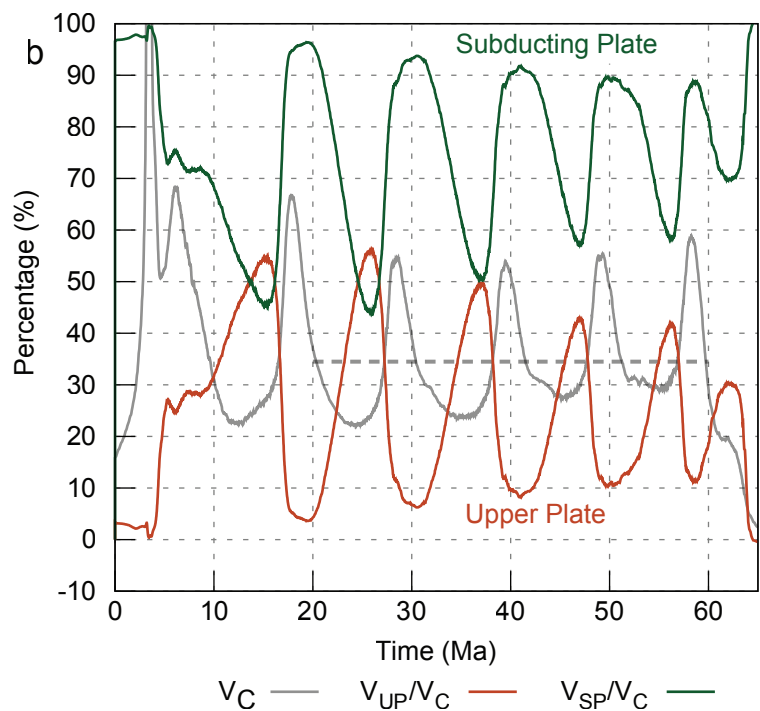
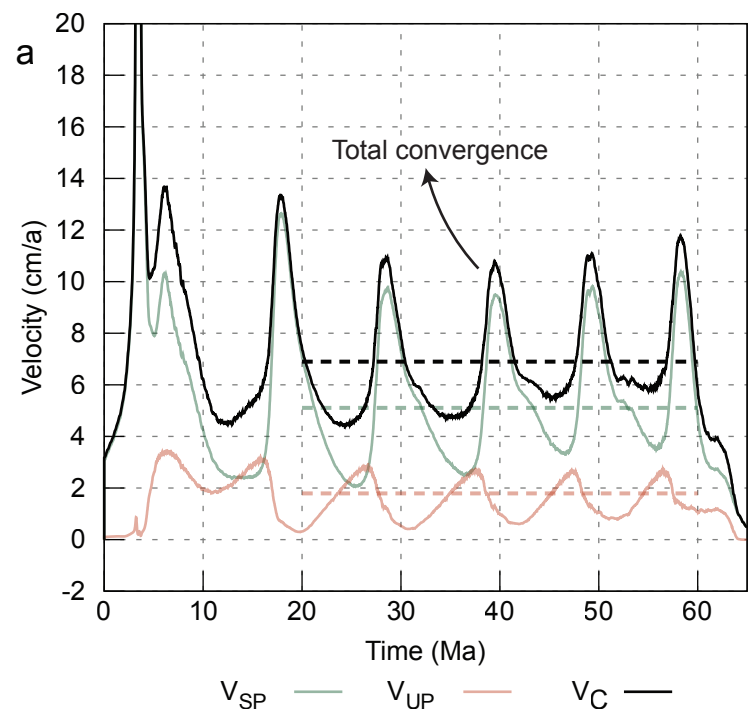




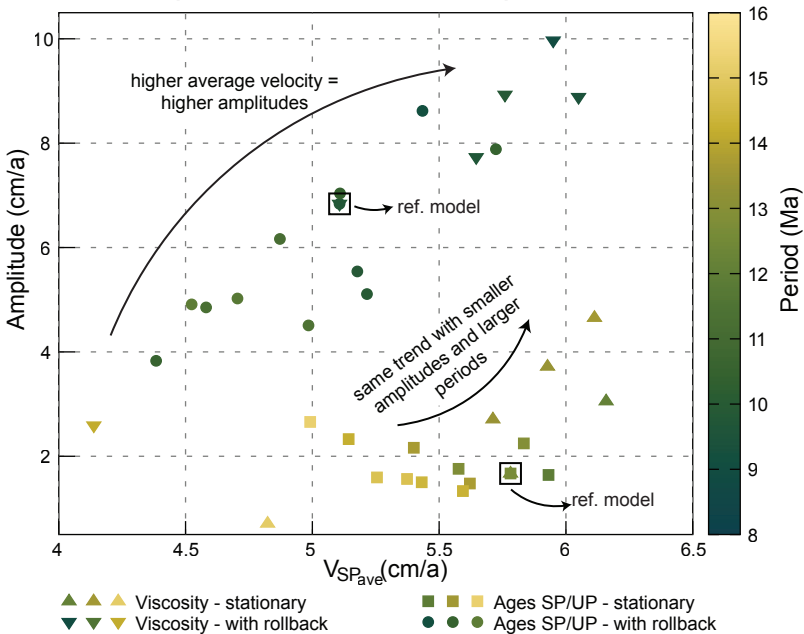








# Amplitude and Period of plate motion



# Effect of plate ages

# Effect of crustal viscosity

